Shadow-Frugal Expectation-Value-Sampling Variational Quantum Generative Model

Kevin Shen, $^{1,\,2,\,3,\,*}$ Andrii Kurkin, $^{1,\,3,\,2}$ Adrián Pérez Salinas, $^{1,\,4}$ Elvira Shishenina, $^{3,\,\dagger}$ Vedran Dunjko, $^{1,\,2}$ and Hao Wang $^{1,\,2}$ $^{1}\langle aQa^L\rangle$ Applied Quantum Algorithms, Leiden University, The Netherlands $^{2}LIACS$, Leiden University, Niels Bohrweg 1, 2333 CA, Leiden, The Netherlands ^{3}BMW Group, 80788 München, Germany

⁴Instituut-Lorentz, Leiden University, Niels Bohrweg 2, 2333 CA, The Netherlands (Dated: December 24, 2024)

Expectation Value Samplers (EVSs) are quantum-computer-based generative models that can learn high-dimensional continuous distributions by measuring the expectation values of parameterized quantum circuits regarding selected observables. However, such models may require unaffordable quantum resources for good performance. This work explores the impact of observable choices on the EVS. We introduce an Observable-Tunable Expectation Value Sampler (OT-EVS). The resulting model provides enhanced expressivity as compared to standard EVS. By restricting our selectable observables, it is possible to use the classical shadow measurement scheme to reduce the sample complexity of our algorithm. We further propose an adversarial training method adapted to the needs of OT-EVS. This training prioritizes classical updates of observables, minimizing the more costly updates of quantum circuit parameters. Numerical experiments confirm our model's expressivity and sample efficiency advantages compared to previous designs, using an original simulation technique for correlated shot noise. We envision our proposal to encourage the exploration of continuous generative models running with few quantum resources.

I. INTRODUCTION

Generative modeling is the task of, given a dataset, learning to generate similar new data. Generative models such as variational autoencoders [1], diffusion probabilistic models [2], and generative adversarial networks (GANs) [3] have achieved remarkable success in various industrial applications, shaping diverse aspects of our daily lives. However, these models face challenges associated with high computational demands and sustainability concerns [4, 5]. As promising alternatives, generative models based on quantum computers have been investigated with some proven advantages for specific artificial problems [6–8]. In this domain, numerous proposals [9] have emerged, such as the Quantum Boltzmann Machine [10–12] and the Quantum Circuit Born Machine [13–15]. In nearly all cases, the models allow the modeling of discrete distributions.

The Expectation Value Sampler (EVS) [16–18] is a comparatively less explored quantum generative model which, in contrast to previous examples, natively models continuous distributions. The generated data emerge as expectation values of preselected observables measured on a state sampled from a particular distribution. Since the proposal of EVS, there have been some studies exploring its integration with classical neural networks in a hybrid quantum GANs framework [19, 20], as well as benchmarking [21, 22] for the applications to image synthesis [23–26] and molecule design [27, 28]. Yet, many questions regarding the theoretical properties of EVS remain unsolved. In particular, the choice of observables, a key component of EVSs, has remained mostly unaddressed.

In this work, we analyze the role of observables and propose an enhanced EVS model with tunable observables. The choice of tunable observables is motivated to enable a trade-off between quantum and classical computational resources without losing performance. We provide two results in this direction. First, we show that our tunable-observable models have higher expressivity than fixed-observable models. That is, the set of reachable probability distributions expands. Second, we design a specific observable parameterization that uses classical shadows [29] to reduce the sample complexity of our model. The considered observables are Pauli strings with low locality, forming a linear space of dimension super-polynomial in the qubit number.

We devise a tailored training method for OT-EVS inspired by adversarial training [3, 30, 31]. The key idea of the training is to update the tunable observables more frequently than the parameters defining the quantum circuit. Since updating the observables requires only classical computation, this can be done without extra quantum measurements. We conduct numerical experiments to benchmark our adapted training method and observe their generally better performances than standard adversarial training for the same amount of quantum resources. In our experiments,

^{*} kevin.shen@bmwgroup.com

[†] Now at Quantinuum, Leopoldstrasse 180, 80804 München, Germany.

we also observe that moderate shot noise levels generally enhance training performances, indicating practical sample efficiency during training. We attribute this phenomenon to a quantum analogue to the regularization induced by artificially injected Gaussian noises in classical GANs [32–38].

The paper is structured as follows. In Section II, we give relevant background on EVS, estimation of expectation values, and adversarial training. Then, in Section III, we formally propose OT-EVS and discuss its expressivity and sample efficiency. Section IV introduces the adapted training algorithm and discusses its sample complexity and shot noise effects. Section V provides numerical experiments that illustrate the performances of OT-EVS. Finally, we close with a discussion in Section VI.

II. BACKGROUND

A. Expectation Value Sampler

EVSs are generative models built on parameterized quantum circuits (PQCs) [39–41], designed for learning continuous distributions. EVSs belong to the class of latent variable models, meaning that data are generated by transforming from some latent random variables. In particular, latent variables are embedded as the gate parameters of some PQC to prepare a random quantum state. The generated data is the expected values of some observables measured on that state, which form a random vector.

Definition 1 (Expectation Value Sampler, adapted from [18]). An Expectation Value Sampler is a generative model specified by a triple of constructive components $(\mathbb{P}_z, U_{\theta}, (O_m)_{m=1}^M)$. \mathbb{P}_z is the distribution of some efficiently samplable latent variable z. U_{θ} is some n-qubit PQC, parameterized by some $\theta \in \Theta \subset \mathbb{R}^d$, that prepares a state $|\psi_{\theta}(z)\rangle = U_{\theta}(z)|0\rangle^{\otimes n}$. $(O_m)_{m=1}^M$ are some observables defined on the same n-qubit system. U_{θ} and $(O_m)_{m=1}^M$ together build a parametric family of functions G_{θ} that transforms \mathbb{P}_z into the output distribution \mathbb{P} . In particular, G_{θ} writes

$$G_{\theta}: \mathcal{Z} \longrightarrow \mathcal{Y}$$

$$\mathbf{z} \longmapsto \mathbf{y} = (\langle \psi_{\theta}(\mathbf{z}) | O_m | \psi_{\theta}(\mathbf{z}) \rangle)_{m-1}^{M},$$

$$\tag{1}$$

where $\mathcal{Z} \subset \mathbb{R}^K$ and $\mathcal{Y} \subset \mathbb{R}^M$ are the supports of \boldsymbol{z} and \boldsymbol{y} respectively. In sampling mode, the Expectation Value Sampler repeatedly draws $\boldsymbol{z} \sim \mathbb{P}_z$ and returns the transformed sample $G_{\boldsymbol{\theta}}(\boldsymbol{z}) \sim \mathbb{P}$ as output.

We consider latent variables that follow a uniform distribution $\mathbb{P}_z = \mathcal{U}([-\pi, \pi]^K)$ throughout this work for simplicity. By fixing \mathbb{P}_z , we will then denote an EVS by its function family G_{θ} .

An interesting property of EVSs is that the output dimension M and the number of qubits n are not intrinsically bound to each other but should be separately determined based on the learning task. EVSs of as few as $\Theta(\log(M))$ qubits are proven to be universal approximators for M-dimensional distributions [18], if U_{θ} takes infinite circuit depth. This finding underscores the capability of EVSs to learn high-dimensional distributions with few qubits.

B. Expection Value Estimation

A core subroutine of EVSs is the computation of many expectation values. In an actual implementation, expectation values can only be estimated through measurements. Each measurement outputs a random outcome, whose distribution is governed by the Born rule [42]. The expectation values are then estimated by processing the measurement outcomes on multiple copies of the quantum state.

Consider estimating the expectation value of an observable O on a state $|\psi\rangle$, $\langle O\rangle = \langle \psi|O|\psi\rangle$. The most general procedure is to prepare multiple copies of $|\psi\rangle$, apply to each copy the circuit that diagonalizes O in the standard measurement basis of the experimental device, and perform the measurement. The expectation value is unbiasedly estimated within accuracy $\mathcal{O}_p(1/\sqrt{N_c})$, N_c being the number of measurements, by averaging measurement results. Two expectation values $\langle O_1 \rangle$ and $\langle O_2 \rangle$ can be estimated simultaneously if $[O_1, O_2] = 0$.

Consider now sparse observables, that is, those having $\mathcal{O}(\text{poly}(n))$ nonzero terms in the Pauli basis decomposition. One can estimate the expectation values of such observables by independently measuring each Pauli string and then summing the contributions [43]. Many improvements to this method have been proposed [44, 45]. One can, for instance, group Pauli strings into commuting sets and perform simultaneous measurements [46, 47]. However, the grouping of Pauli strings is non-unique, and the optimal grouping concerning sample efficiency is an NP-hard problem, for which heuristic solutions have been extensively studied [48–52]. One can also perform importance sampling to flexibly distribute measurements among Pauli strings according to their coefficients [46, 53].

More recently, the measurement scheme of classical shadows [29] has raised significant attention. Classical shadows are conducted by first repeatedly measuring the state $|\psi\rangle$ in randomly chosen bases. The measurement outcomes can be post-processed to simultaneously yield estimations of the expectation values of many observables. This matches the needs of EVSs. Among all variants of classical shadows, the most studied case is when all observables are k-local Pauli strings. One can estimate the expectation values of L different maximally k-local Pauli observables, each to accuracy ϵ , with

$$N_s \in \mathcal{O}\left(\frac{3^k \log L}{\epsilon^2}\right) \tag{2}$$

copies of $|\psi\rangle$ [29] with high probability. It is common to require $k \in \mathcal{O}$ (polylog(n)) to match the standard sample efficiency. The sample complexity in classical shadows can be further improved by adopting a locally-biased distribution of measurement bases [54] or applying derandomization techniques [55], given more knowledge on the observables to measure.

C. Adversarial Training

Generative models need to be trained before generating useful data. Many early generative models, best represented by Boltzmann machines [56, 57], provide explicit access to the likelihood function and can be trained by maximizing that function. The training is equivalent to minimizing the Kullback-Leibler divergence between the generator's output distribution \mathbb{P} and the target distribution \mathbb{Q} .

Definition 2 (KL-divergence [58]). Assume a probability space $(\mathcal{X}, \mathcal{A}, \mu)$. The Kullback-Leibler divergence between two absolutely continuous $(w.r.t. \ \mu)$ probability distributions \mathbb{P} and \mathbb{Q} is defined as:

$$\mathcal{D}_{KL}(\mathbb{P} \parallel \mathbb{Q}) = \int_{\mathcal{X}} p(x) \log \left(\frac{p(x)}{q(x)} \right) d\mu(x), \tag{3}$$

where $p = \frac{d\mathbb{P}}{d\mu}$ and $q = \frac{d\mathbb{Q}}{d\mu}$ are the densities of \mathbb{P} and \mathbb{Q} .

However, likelihood functions are intractable for many generative models. Nevertheless, \mathcal{D}_{KL} is still widely used as an evaluation metric for generative models after training [59–62]. We will also use \mathcal{D}_{KL} for evaluation later in our numerical experiments.

Adversarial training thus arose as a practical alternative to likelihood maximization [3]. In the adversarial framework, the generative model is trained alternatingly with a competing agent called the *critic* (or discriminator). The competing training allows one to improve both agents. The critic is trained to better distinguish the generated data from real data, and the generative model is trained to capture the real data distribution. A particular example of adversarial training is the Wasserstein GAN (WGAN) [30, 31], which, in principle, minimizes the Wasserstein-1 distance in training.

Definition 3 (Kantorovich-Rubenstein duality [63]). Wasserstein-1 distance between two probability distributions \mathbb{P} and \mathbb{Q} in \mathbb{R}^m is:

$$W_1(\mathbb{P}, \mathbb{Q}) = \sup_{\|D\|_L \le 1} \left(\int_{\mathcal{X}} D(x) d\mathbb{P} - \int_{\mathcal{Y}} D(y) d\mathbb{Q} \right), \tag{4}$$

where \mathcal{X} and \mathcal{Y} are the supports of \mathbb{P} and \mathbb{Q} , and the supremum is taken over the set of 1-Lipschitz functions D.

The above variational problem is tackled by considering a parametrized function of D in WGAN.

III. OBSERVABLE-TUNABLE EXPECTATION VALUE SAMPLER

The main contribution of this manuscript is the Observable-Tunable Expectation Value Sampler (OT-EVS). This model extends the one described in Definition 1, where we use fixed observables.

Definition 4 (Observable-Tunable Expectation Value Sampler (OT-EVS)). An Observable-Tunable Expectation Value Sampler is a generative model specified by a quadruple of constructive components $(\mathbb{P}_z, U_{\boldsymbol{\theta}}, (O_l)_{l=1}^L, \boldsymbol{\alpha})$. The quantity $\boldsymbol{\alpha} \in \mathbb{R}^{M \times L}$ is a tunable weight matrix. For every fixed $\boldsymbol{\alpha}$, the generative model is given by the EVS specified via the triple $(\mathbb{P}_z, U_{\boldsymbol{\theta}}, (\sum_{l=1}^L \boldsymbol{\alpha}_{m,l} O_l)_{m=1}^M)$.

In this paper, the regular EVS given in Definition 1 will be called Observable-Fixed (OF)-EVS to make the difference explicit. The Definition 4 allows us to interpret OT-EVS as a generalization of OF-EVS constructed by linear combinations. This choice is made to accurately assess the independent contributions of the model's quantum (EVS) and classical (linear combination) components. Other previous proposals to improve EVSs considered more general classical postprocessing, for instance, by feeding the outputs of EVSs into classical deep learning modules [23, 24, 26]. These models are, however, hard to analyze in the look for quantum advantages due to the relevant role that the classical components can have on the performance of the model.

A. Tunable Observables Enhance Expressivity

We recall that constructing an EVS as a universal generative model requires infinite-depth circuits [18]. However, efficient quantum computation (BQP) only permits circuits of depth $\mathcal{O}(\text{poly}(n))$. Therefore, EVSs will inevitably have restricted expressivity in practice. The choice of observables will then be critical for model expressivity and, hence, learning performance. We will show that, in general, an OT-EVS is more expressive than its analogous OF-EVS, ceteris paribus. Let us start with formally defining the notion of relative expressity.

Definition 5 (Relative Expressivity). Let G_{θ} and H_{ϕ} be two parametric families of random variables with finite variances. We define $S_G := \{G_{\theta} : \mathbb{R}^K \to \mathbb{R}^M | \theta \in \mathbb{R}^d \}$ and S_H similarly. We say

- (i) G_{θ} is at least as expressive as H_{ϕ} , if $\forall h \in S_H$, $h \in S_G$. We write $H_{\phi} \preceq G_{\theta}$. \preceq is a non-strict order.
- (ii) G_{θ} is strictly more expressive than H_{ϕ} , if $H_{\phi} \leq G_{\theta}$ and $\exists g \in S_G$, $g \notin S_H$. We write $H_{\phi} \prec G_{\theta}$. \prec is a strict partial order.
- (iii) G_{θ} is as expressive as H_{ϕ} , if $H_{\phi} \leq G_{\theta}$ and $G_{\theta} \leq H_{\phi}$. We write $H_{\phi} \cong G_{\theta}$. \cong is the identity relation.

A few statements then follow naturally.

Proposition 1 (Expressivity never decreases using tunable observables). For any OF-EVS $H_{\theta} := (\mathbb{P}_z, U_{\theta}, (Q_m)_{m=1}^M)$ and any OT-EVS $G_{\theta,\alpha} := (\mathbb{P}_z, U_{\theta}, (O_l)_{l=1}^L, \alpha)$,

$$\forall 1 \le m \le M, \exists 1 \le l \le L, Q_m = O_l \implies H_{\phi} \le G_{\theta} \tag{5}$$

Proposition 2 (Expressivity of a universal generative model cannot increase further). For any OF-EVS $H_{\theta} := (\mathbb{P}_z, U_{\theta}, (Q_m)_{m=1}^M)$ and any OT-EVS $G_{\theta, \alpha} := (\mathbb{P}_z, U_{\theta}, (O_l)_{l=1}^L, \alpha)$,

$$G_{\theta,\alpha}$$
 is universal and $\forall 1 \le m \le M, \exists 1 \le l \le L, Q_m = O_l \implies H_{\phi} \cong G_{\theta}$ (6)

Despite the existence of the extremal case of universal EVS depicted in Proposition 2, OT-EVSs will generally be strictly more expressive than their analogous OF-EVSs in practice. We illustrate the reasoning with a simple example.

Example 1. (Toy example) Consider the two-qubit circuit $U_{\theta}(z) = R_Y(z_1 + \theta_1) \otimes R_Y(z_2 + \theta_2)$ with $z_1, z_2 \sim \mathbb{P}_z = \mathcal{U}[-\pi, \pi]$ and $\theta_1, \theta_2 \in \mathbb{R}$. Consider the OF-EVS $H_{\theta} := (\mathbb{P}_z, U_{\theta}, (O_1, O_2))$, where $O_1 = X_1I_2$ and $O_2 = I_1X_2$, and the OT-EVS $G_{\theta,\alpha} := (\mathbb{P}_z, U_{\theta}, (O_1, O_2), \alpha)$, where $\alpha \in \mathbb{R}^{2 \times 2}$. Then $H_{\theta} \prec G_{\theta,\alpha}$.

In Example 1, $(y_1, y_2) = H_{\theta}(z_1, z_2)$ writes

$$y_m = \sin\left(\frac{\theta_m + z_m}{2}\right) \quad \text{for } m \in \{1, 2\},\tag{7}$$

while $G_{\theta,\alpha}(z_1, z_2) = (\alpha_{11}y_1 + \alpha_{12}y_2, \alpha_{21}y_1 + \alpha_{22}y_2)$. We can attribute the increase in expressivity to two causes. First, $G_{\theta,\alpha}$ is not closed under convolution. That is, linear combinations of y_1 and y_2 follow different distributions as y_1 or y_2 in general, even though y_1 and y_2 are identically distributed up to θ . Second, $\alpha_{11}y_1 + \alpha_{12}y_2$ is in general correlated with $\alpha_{21}y_1 + \alpha_{22}y_2$, while y_1 and y_2 themselves are always independent.

For other EVSs with more complex circuits and observables, expressivity generally increases for similar reasons. We illustrate this further in numerical experiments in Section V C. Here we analyze one more characteristic example, in which the PQC accumulates too much randomness from z such that $U_{\theta}(z)|0\rangle$ becomes Haar-random $\forall \theta \in \Theta$.

Example 2. (Haar-random circuit) Consider an OF-EVS $H_{\theta} := (\mathbb{P}_z, U_{\theta}, (O_1))$ that $\forall \theta \in \Theta, U_{\theta}(z)|0\rangle$ follows the Haar-random distribution over n-qubit quantum states, n > 1. Consider an OT-EVS $G_{\theta,\alpha} := (\mathbb{P}_z, U'_{\theta}, (O_1, O_2), \alpha)$, where $\alpha \in \mathbb{R}^{1 \times 2}$, satisfying the constraint

$$\forall V \in \mathcal{SU}(2^n), \quad VO_1V^{\dagger} \neq O_2. \tag{8}$$

Then $H \prec G$.

To show the validity of the previous arguments, we use existing theoretical tools [64]. When measuring a Haarrandom state, the expectation value of a given observable O is a random variable stemming from the inner product of a symmetric Dirichlet random variable and the eigenvalues of the observable. Consider an observable O_{α} given by weighted sums of O and some other observables. The eigenvalues of O_{α} will depend on the spectra of all constituent observables and their weights. Hence, both the resulting spectrum and the underlying distribution of the expectation value differ from those of O originally.

B. The Shadow-Frugal Parameterization

We consider parametrizing the observables as weighted sums of maximally k-local Pauli operators, which allows for efficient estimation of the expected values using classical shadows, given that the locality k is bounded. We call this parameterization the *shadow-frugal parameterization*.

Definition 6 (Shadow-Frugal Parameterization). Consider an OT-EVS ($\mathbb{P}_z, U_{\theta}, (P_l)_{l=1}^L, \alpha$). Its observables are in shadow-frugal parameterization if all P_l are k-local Pauli strings, where $k \in \mathcal{O}(\operatorname{polylog}(n))$.

In actual implementation, one can leverage the classical shadows with measurements in randomized single-qubit Pauli bases. A total number of

$$N_s \in \mathcal{O}\left(\frac{3^k \log L}{\epsilon^2}\right) \tag{9}$$

measurements are sufficient to estimate the expectation values of all L Pauli strings [55] with accuracy $\epsilon > 0$ with high probability. To obtain the output data, we combine the expectation values according to α .

In our context, the number of k-local Pauli strings, for $k \in \mathcal{O}(\text{polylog}(n))$, scales as

$$L = \sum_{j=0}^{k} \binom{n}{j} 3^j \in 2^{\tilde{\Theta}(\log(n)^c)}. \tag{10}$$

Inserting (10) into (9) shows that a total $\mathcal{O}(\text{poly}(n)/\epsilon^2)$ measurements are sufficient to estimate the super-polynomially many Pauli strings, which suggests the sample efficiency of the shadow-frugal OT-EVS.

IV. TRAINING AND SAMPLING

A. Adapted Adversarial Training

We consider OT-EVS training based on the WGAN framework [31]. We discuss how this training procedure can be adapted to improve resource efficiency, that is, giving priority to spending classical resources while saving quantum resources

As previously mentioned, WGAN requires two networks: the generator, which transforms a prior distribution \mathbb{P}_z into the distribution \mathbb{P} that approximates the target distribution \mathbb{Q} , and the critic, which serves as the function D in estimating $\mathcal{W}_1(\mathbb{P},\mathbb{Q})$. The same approach can be applied to an OT-EVS $G_{\theta,\alpha}$, which now becomes the generator. We could, in principle, use a PQC as a critic, similar to the quantum discriminator in vanilla QGANs [16, 23??]. However, in this work, we utilize classical networks as critics to focus on the aspects of the generator.

Loss functions govern the optimization pipeline for optimizing the generator and the critic. The generator loss function \mathcal{L}_G is given by

$$\mathcal{L}_{G}(\boldsymbol{\theta}, \boldsymbol{\alpha}; \boldsymbol{w}) = -\frac{1}{B} \sum_{i=1}^{B} D_{\boldsymbol{w}}(\boldsymbol{y}^{(i)}), \tag{11}$$

where B is the batch size, $D_{\boldsymbol{w}}(\cdot)$ is the critic neural network and $\boldsymbol{y}^{(i)} = G_{\boldsymbol{\theta},\alpha}(\boldsymbol{z}^{(i)})$ are samples outputted from the generator. The two sets of parameters $\boldsymbol{\theta}$ and $\boldsymbol{\alpha}$ are updated via stochastic gradient descent with respect to \mathcal{L}_G . For each update, a batch of latent variables, $\{\boldsymbol{z}^{(i)} \sim \mathbb{P}_z \mid 1 \leq i \leq B\}$, are needed.

For the critic, we adopted the gradient penalty method [31], which softly constrains the critic network $D_{\boldsymbol{w}}$ to be a 1-Lipschitz function:

$$\mathcal{L}_{C}(\boldsymbol{w};\boldsymbol{\theta},\boldsymbol{\alpha}) = \frac{1}{B} \sum_{i=1}^{B} \left[D_{\boldsymbol{w}}(\boldsymbol{y}^{(i)}) - D_{\boldsymbol{w}}(\boldsymbol{x}^{(i)}) + \lambda \left(\left\| \nabla_{\hat{\boldsymbol{x}}} D_{\boldsymbol{w}}(\hat{\boldsymbol{x}}^{(i)}) \right\|_{2} - 1 \right)^{2} \right], \tag{12}$$

where $\boldsymbol{x}^{(i)}$ are training data, $\lambda > 0$ is a regularization constant and $\hat{\boldsymbol{x}}^{(i)} = \varepsilon \boldsymbol{x}^{(i)} + (1 - \varepsilon) \boldsymbol{y}^{(i)}$, with $\varepsilon \sim \mathcal{U}[0, 1]$, are random vectors interpolated between training data and the generated data. The last term is a regularization term that penalizes $D_{\boldsymbol{w}}$ with large Lipschitz constants, so that \mathcal{L}_C approximates $-\mathcal{W}_1(\mathbb{P}, \mathbb{Q})$ (Definition 3). The parameters \boldsymbol{w} are updated via stochastic gradient descent with respect to \mathcal{L}_C . For each update, a batch of latent variables, $\{\boldsymbol{z}^{(i)} \sim \mathbb{P}_z \mid 1 \leq i \leq B\}$, as well as a batch of training data $\{\boldsymbol{x}^{(i)} \sim \mathbb{Q} \mid 1 \leq i \leq B\}$ are needed.

Updates of $\boldsymbol{\theta}$, $\boldsymbol{\alpha}$ or \boldsymbol{w} require different amounts of quantum resources. Each update of \boldsymbol{w} takes N_sB copies of quantum states, where N_s denotes the number of copies for generating each piece of data $\boldsymbol{y}^{(i)}$ in a batch. This number is independent of the dimension of \boldsymbol{w} , because $\partial_{\boldsymbol{w}}\mathcal{L}_C$ is computable by classical backpropagation [65]. For the same reason, each update of $\boldsymbol{\alpha}$ also takes N_sB copies. In contrast, each update of $\boldsymbol{\theta}$ involves $2N_dN_sB$ copies, where N_d is the dimension of $\boldsymbol{\theta}$, because $\partial_{\boldsymbol{\theta}}\mathcal{L}_G$ needs to be computed by performing the parameter shift rule [66, 67] on the quantum computer.

Gradient	Quantum Resources
$\partial_{m{w}} \mathcal{L}_C$	$N_s B$
$\partial_{m{lpha}} \mathcal{L}_G$	$N_s B$
$\partial_{m{ heta}} \mathcal{L}_G$	$2N_dN_sB$

Table I. The number of copies of quantum states required for each update of the critic parameters \boldsymbol{w} , the circuit parameters $\boldsymbol{\theta}$ and the observable parameters $\boldsymbol{\alpha}$. \mathcal{L}_C and \mathcal{L}_G are the critic loss function (Equation 12) and the generator loss function (Equation 11). N_s is the cost of each piece of data in a batch. B is the batch size. N_d is the dimension of the circuit parameters.

The main idea behind our adaptations is to minimize the usage of quantum resources and compensate for it with more classical resources that are generally less expensive in energy and time. We achieve this by increasing the frequency of updating α compared to θ . We propose two different variants, which we denote as Asynchronous (Async.) and Decoupled (Decoup.) respectively. We denote the default method in which α and θ are not distinguished as Joint. We highlight their differences below and provide the complete pseudocodes in Appendix A.

- (1) Joint: α are updated simultaneously with θ . Each training iteration makes first $N_{\boldsymbol{w}} \geq 1$ updates to \boldsymbol{w} and then one update to θ and α simultaneously.
- (2) Asynchronous: α are updated together with θ , but more frequently. In each training iteration, the updates to w remain the same as in Joint. After that, α is updated for $N_{\alpha} > 1$ times, and then θ is updated once.
- (3) Decoupled: α are updated simultaneously with w. Each training iteration begins with N_{α} loops, each consisting of $\lceil N_w/N_{\alpha} \rceil$ updates to w and then one update to α . After all loops, θ will be updated once.

One can check that all three variants take similar quantum resources per training iteration when $N_d \gg 1$. However, the *Asynchronous* and *Decoupled* variants allow for enhanced adaptability of the classically updated observables, potentially saving the need for quantum calls. Based on this reasoning, we formulate

Hypothesis 1. The two variants Asynchronous and Decoupled, in which the observable parameters α become more frequently updated, generally outperform the default Joint method for the same amount of quantum resources.

This hypothesis will be verified through numerical experiments in Section VB.

Finally, we remark that we chose to adapt the training methods from the framework of WGAN [30] due to its relatively good performance in the classical case and popularity in quantum literature [25, 26]. However, the adaptations we propose can be easily generalized to other adversarial training frameworks [35, 37], which have competitive or even superior performances to WGAN in some situations [68] in the classical case. We leave it for future studies to investigate which framework works the best for OT-EVS generators.

B. Shot Noise and Sample Complexity

We have previously neglected shot noise in the training of OT-EVS. However, in actual implementation, shot noise is always present in expectation value estimation, which perturbs the evaluation of loss functions.

Consider now an arbitrary training iteration. We denote the empirical distribution for the drawn batch of training samples $(\boldsymbol{x}^b)_{b=1}^B$ by \mathbb{Q}^B . Analogously, we denote the empirical distribution for the ideally generated samples $(\boldsymbol{y}^b)_{b=1}^B$ by \mathbb{P}^B , i.e., if there were no shot noise. Because of finite measurements, what we actually have are the shot-noise-perturbed generated samples $(\tilde{\boldsymbol{y}}^b)_{b=1}^B$, whose empirical distribution we denote by $\tilde{\mathbb{P}}^B$.

The training objective is to minimize $W_1(\mathbb{P}^B, \mathbb{Q}^B)$, which can only be approximated by $W_1(\tilde{\mathbb{P}}^B, \mathbb{Q}^B)$. Triangle inequality suggests that the approximation accuracy is bounded by $W_1(\mathbb{P}^B, \mathbb{P}^B)$,

$$\left| \mathcal{W}_1(\mathbb{P}^B, \mathbb{Q}^B) - \mathcal{W}_1(\tilde{\mathbb{P}}^B, \mathbb{Q}^B) \right| \le \mathcal{W}_1(\mathbb{P}^B, \tilde{\mathbb{P}}^B). \tag{13}$$

We will now analyze the number of measurements needed to suppress $W_1(\mathbb{P}^B, \tilde{\mathbb{P}}^B)$ to some target level $\epsilon > 0$. We compare the resource required by the classical shadow measurement scheme to that of the conventional one (Section II). We only consider the vanilla versions of each method since most improved versions require optimizations based on the measured state $|\psi\rangle$ and the observable parameters α , complicating the analysis.

Theorem 1 (Sample Complexity per Training Iteration). Let L be the number of k-local Pauli strings whose expectation values are to be estimated. Let B be the batch size. Let \mathbb{P}^B be the noiseless empirical distribution of a batch of generated samples from an OT-EVS under the shadow-frugal parameterization, and $\tilde{\mathbb{P}}^B$ be its noise-perturbed estimation and let $\|\mathbf{\alpha}\|_{\infty} \leq T$. Then

$$\Pr\left(\mathcal{W}_1(\mathbb{P}^B, \tilde{\mathbb{P}}^B) \le \epsilon\right) > 1 - \delta \tag{14}$$

is achieved if the total number of measurements N_s satisfy

$$N_s \ge \left\lceil 68 \frac{T^2 3^k}{\epsilon^2} \log \left(\frac{2BL}{\delta} \right) \right\rceil B \tag{15}$$

or

$$N_s \ge \left\lceil 2\frac{T^2}{\epsilon^2} \log \left(\frac{2BL}{\delta}\right) \right\rceil BL \tag{16}$$

when using the classical-shadow or the conventional measurement scheme respectively.

We remark that the condition $\|\alpha\|_{\infty} \leq T$ implies $\|O_m\|_{\infty} \leq T$, $\forall 1 \leq m \leq M$.

Theorem 1 suggests that the classical shadows measurement scheme shows a super-polynomial resource advantage over the conventional measurement scheme for training shadow-frugal OT-EVS when $k \in \mathcal{O}(\text{polylog}(n))$. We thus formulate a hypothesis to be numerically verified in Section VB.

Hypothesis 2. Using the classical shadow measurement scheme to training the shadow-frugal OT-EVS generally requires much fewer measurements than the conventional measurement scheme to achieve the same training performance for all three variants of adversarial training.

The remaining question is, to what size $W_1(\mathbb{P}^B, \tilde{\mathbb{P}}^B)$ should be bounded. Increasing this bound will decrease sample complexity and, subsequently, the cost of training OT-EVS. On one hand, $W_1(\mathbb{P}^B, \tilde{\mathbb{P}}^B)$ must not be overlarge. Otherwise, $W_1(\mathbb{P}^B, \mathbb{Q}^B)$ cannot be accurately approximated and the training cannot converge. On the other hand, making $W_1(\mathbb{P}^B, \mathbb{Q}^B)$ arbitrarily small does not necessarily yield the best training performance either. We hypothesize that a moderate size of $W_1(\mathbb{P}^B, \tilde{\mathbb{P}}^B)$ may generally benefit the training.

Hypothesis 3. Injecting noise has been shown to ameliorate training instability or mode collapse issues for classical GANs [32–38]. We conjecture that a moderate number of measurements introduces a shot-noise-induced regularizer, which improves the training performance of OT-EVS.

We will verify Hypothesis 3 with numerical experiments in Section VB.

V. NUMERICAL EXPERIMENTS

To investigate the training behavior of OT-EVS, we conduct a series of controlled experiments in which an OT-EVS with randomly chosen parameters generates the training dataset, and an identical OT-EVS is randomly initialized and learns the distribution, in a similar vein to Ref. [16]. In these experiments, the models are thus always guaranteed sufficient expressivity to represent the target distribution exactly, although the training may still face challenges. Therefore, the experiments constitute a testbed for comparing the performances of different variants of adversarial training and analyzing the impact of shot noise.

To efficiently but also accurately simulate the training of OT-EVS at a large scale, we derive the shot noise from classical shadows up to the second moment, with dependence on the measured state, and in a way compatible with automatic differentiation (Appendix C).

To our knowledge, with this simulation technique, we are the first to simulate a quantum machine learning (QML) algorithm in which classical shadows participate in the computation of gradients. This is different from previous classical-shadows-enhanced QML algorithms [69–73], where classical shadows are used for initial data acquisition only.

Finally, to evaluate the trained models, we use an estimator of $\mathcal{D}_{KL}(\mathbb{P},\mathbb{Q})$ that is based on K-nearest-neighbors [74]. The estimator is efficiently computable using training and generated samples and yields high accuracy even for moderately ($\lesssim 100$) high-dimensional distributions. Appendix D provides other experiment implementation details.

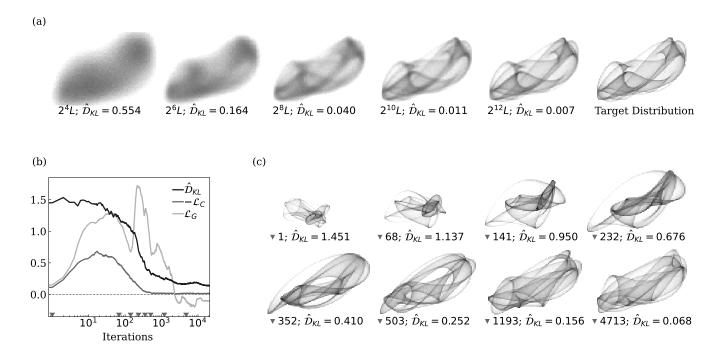


Figure 1. (a) Convolutions of an example 2d target distribution with shot noises from sampling with different finite numbers of measurements (number of measurements and estimated KL-divergences labelled). (b) Example of training curves for the generator loss, the critic loss, and the KL divergence. (c) Generator distributions at selected training iterations, neglecting shot noises (iteration and estimated KL-divergences labelled).

A. Illustrative Example

To illustrate the experiment setup, we consider a small OT-EVS that generates two-dimensional data (Figure 1). First, in Figure 1(a), we visualize the effect of shot noise by comparing the outputs of a generator using finite measurements to those ideal outputs assuming infinite measurements. We repeat the process with different numbers of measurements. The decreasing \hat{D}_{KL} between the shot-noise-perturbed distribution and the ideal distribution aligns well with the increasing sharpness of the probability distribution as more measurements are used.

We keep the previous ideal distribution as the learning target for the next experiment, randomly initialize an identical generator, and show its adversarial training process against a critical neural network. The training curves for $\mathcal{L}_G(\tilde{\mathbb{P}}^B, \mathbb{Q}^B)$, $\mathcal{L}_C(\tilde{\mathbb{P}}^B, \mathbb{Q}^B)$ and $\hat{\mathcal{D}}_{KL}(\mathbb{P} \parallel \mathbb{Q})$ are plotted in Figure 1(b), and snapshots of the process are shown in Figure 1(c). We remark that $\mathcal{L}_C(\tilde{\mathbb{P}}^B, \mathbb{Q}^B)$ has converged to 0, despite the visible difference between the histograms of \mathbb{P} and \mathbb{Q} , indicating that critic fails to estimate $\mathcal{W}_1(\tilde{\mathbb{P}}^B, \mathbb{Q}^B)$ at the later stage, most likely due to limited expressivity of the critic. In contrast, $\hat{\mathcal{D}}_{KL}(\mathbb{P} \parallel \mathbb{Q})$ captures the model performance better, reflected by its strong correlation with the visual similarity between the probability distributions of \mathbb{P} and \mathbb{Q} during training.

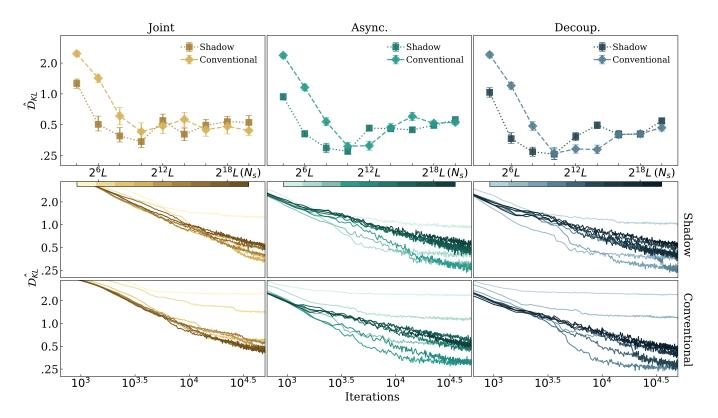


Figure 2. Selected experiment (sequential ansatz at small configuration) for comparing the three variants of training for OT-EVS under the classical shadows or conventional measurement scheme with different numbers of measurements. The top graphs show the interquartile mean and bootstraped 95% confidence intervals over 20 trials for the estimated KL-divergences at 50k iterations. The bottom graphs show the corresponding interquartile mean training trajectories.

B. Training Methods and Shot Noise

The next experiments compare the three variants of training (Section IV A) under the classical shadows and conventional measurent schemes with varying numbers of measurements. To ensure the generality of our results, we examine two common ansatze in QML literature: a sequential ansatz and a brickwork ansatz (Appendix D). However, we do not advocate their usage for practical applications. We examine models constructed with both ansatze across three scales with different qubit numbers (n), layers (N_l) , locality (k), and output dimension of the model (M):

- (1) n = 8, $N_l = 2$, k = 1, M = 8 (small configuration),
- (2) $n = 8, N_l = 9, k = 1, M = 8$ (deeper configuration),
- (3) n = 11, $N_l = 2$, k = 2, M = 64 (wider configuration).

For each model, we conduct 20 independent experiment trials. The model is randomly instantiated and sampled in each trial to produce the training dataset. Then, an identical model is randomly initialized and trained for 50k iterations using each of the three training variants under each measurement setting. The same initial parameters and hyperparameters are used for all combinations of training variant and measurement setting in each trial. The final $\hat{\mathcal{D}}_{KL}(\mathbb{P} \parallel \mathbb{Q})$ for all runs with the model on sequential ansatz in a small configuration are recorded and summarized in Figure 2. Similar results for other models are provided in Appendix E.

The results here to support our Hypotheses 1, 2, and 3.

C. Tunable versus Fixed Observables

In the final experiments, we compare the training of OT-EVSs to that of OF-EVSs (Figure 3). We isolate the effect of potential trainability issues from the analysis of expressivity.

We first examine the presence of trainability issues common to PQC-based models. We expect both OT-EVS and OF-EVS generally to be less trainable when their circuits are more heavily parameterized, a phenomenon commonly known as the barren plateau [75, 76]. We study both the sequential and brickwork ansatze. For each ansatz, we conduct 20 independent trials. In each trial, we randomly instantiate an OT-EVS at the scale of n = M = 8, $N_l = 1$, k = 1 to produce the training data. We denote this model by H_1^T . Then, we fix the observables and train a sequence of OF-EVSs with circuits of increasingly more layers $N_l \in \{1, 3, ..., 15\}$. We denote these models by $H_{N_l}^F$.

We design both ansatze so that two neighboring layers can conjugate each other when their parameters take certain values. Therefore, $\forall N_l \in \{1, 3, \dots, 15\}$, $H_{N_l}^F$ have sufficient expressivity to learn the target distribution. The learning performance should then purely reveal trainability properties.

Next, we compare the trainability of OT-EVSs to OF-EVSs. We train a sequence of OT-EVSs in each trial by increasing N_l and randomly initializing the observables. We denote these models by $H_{N_l}^T$. We use the *Decoupled* training method.

Then, we study the expressivity gain of the OT-EVS versus its analogous OF-EVS, as a supplement to Section III A, and the extent to which the expressivity gap can be filled if the OF-EVS uses a more expressive circuit. In each trial, we train another sequence of OF-EVSs with the same circuits as $H_{N_l}^F$ and $H_{N_l}^T$, but employing the single-qubit Pauli-Z operators, $(I_{\overline{m}}Z_m)_{m=1}^M$, as the fixed observables. We denote these models by $Z_{N_l}^F$. Z-observables is a standard choice in QGANs literature [16, 17].

We further allow the usage of global scaling and translation to the raw outputs of $Z_{N_l}^F$ for increasing expressivity, which is a common practice in machine learning. We remark that $H_{N_l}^T$ are naturally capable of global rescaling and translation through the tunable observables.

Figure 3 shows the final $\hat{\mathcal{D}}_{KL}(\mathbb{P} \parallel \mathbb{Q})$ for all three model sequences. Looking at $H_{N_l}^T$ and $H_{N_l}^F$, we do not observe the barren plateau phenomenon. $H_{N_l}^T$ seem more trainable than $H_{N_l}^F$ for all $1 \leq N_l \leq 15$, the reason remains unknown. We leave the study of whether using tunable observables generally benefits training for future studies. By comparing $Z_{N_l}^F$ against $H_{N_l}^F$, we observe that more expressive circuits do not fully compensate for the expressivity gap due to the usage of fixed observables.

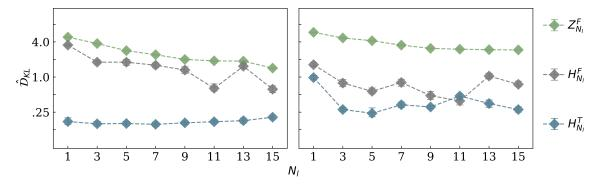


Figure 3. Comparison of the expressivity and trainability between OF-EVSs and their analogous OT-EVSs. Shown are the interquartile mean and bootstraped 95% confidence intervals over 20 trials for the estimated KL-divergences at 50k iterations for the OF-EVSs with Pauli-Z observables, the OF-EVSs with given ideal observables, and the OT-EVSs with increasing layers of the sequential ansatz (left) and brickwork ansatz (right).

VI. DISCUSSION

In this work, we propose a quantum generative model extending the Expectation Value Sampler using tunable observables. The model outputs random variables, given by the expectation values of an internal random state. Ideally, the outcomes follow a target probability distribution accessible through data. The tunable-observable extension enhances the expressivity of the model while reducing the quantum resources required for training, as compared to fixed-observables models. These improvements are demonstrated both analytically and empirically. Our contributions are as follows. a) The expressivity enhancement is demonstrated by showing that fixed-observable models are included in tunable-observable models, but not the converse. b) We can improve sample complexity by restricting our observables to those that can be efficiently estimated using classical shadows. We also provide upper bounds on the number of measurements required to estimate the output probability distribution up to a predefined precision. c) We propose

two new adversarial training procedures with improved performances while maintaining the same requirements of quantum resources, by fine-tuning the update rate of parameters in the observables and in the quantum circuits.

We showcase the performance of tunable-observable models by conducting numerical experiments. First, tunable-observable models in practice outperform fixed-observable models, even in data generated by fixed-observable models. Second, the tailored training procedures, together with the classical-shadow sampling strategy, reduce the overall training cost. Furthermore, the training procedures exhibit an interesting phenomenon: moderate levels of shot noise can improve training performance, similar to the noise injection in classical GAN training.

Interesting foreseeable research directions include investigating the performance of tunable-observable models on low-dimensional, real-world data sets. Technically valuable contributions are theoretical analysis of the convergence properties and stability of the proposed training procedures as well as numerical characterization of the level of shot noise that is beneficial to the model's performance.

ACKNOWLEDGMENTS

KS thanks Riccardo Molteni, Yash Patel, and Susanne Pielawa for insightful discussions. This research was funded by the BMW Group. VD thanks the support of the Dutch National Growth Fund (NGF), as part of the Quantum Delta NL programme. This work was also partially supported by the Dutch Research Council (NWO/OCW), as part of the Quantum Software Consortium programme (project number 024.003.03), and co-funded by the European Union (ERC CoG, BeMAIQuantum, 101124342).

Data availability: Simulation codes are available under reasonable request.

- [1] D. P. Kingma and M. Welling, Auto-Encoding Variational Bayes (2022), arXiv:1312.6114.
- [2] J. Sohl-Dickstein, E. A. Weiss, N. Maheswaranathan, and S. Ganguli, Deep unsupervised learning using nonequilibrium thermodynamics, in *Proceedings of the 32nd International Conference on International Conference on Machine Learning Volume 37*, ICML'15 (JMLR.org, Lille, France, 2015) pp. 2256–2265.
- [3] I. Goodfellow, J. Pouget-Abadie, M. Mirza, B. Xu, D. Warde-Farley, S. Ozair, A. Courville, and Y. Bengio, Generative Adversarial Nets, in *Advances in Neural Information Processing Systems*, Vol. 27 (Curran Associates, Inc., 2014).
- [4] N. C. Thompson, K. Greenewald, K. Lee, and G. F. Manso, The Computational Limits of Deep Learning (2022), arXiv:2007.05558.
- [5] D. Patterson, J. Gonzalez, Q. Le, C. Liang, L.-M. Munguia, D. Rothchild, D. So, M. Texier, and J. Dean, Carbon Emissions and Large Neural Network Training (2021), arXiv:2104.10350.
- [6] X. Gao, Z. Zhang, and L. Duan, An efficient quantum algorithm for generative machine learning (2017), arXiv:1711.02038 [quant-ph, stat].
- [7] B. Coyle, D. Mills, V. Danos, and E. Kashefi, The Born Supremacy: Quantum Advantage and Training of an Ising Born Machine, npj Quantum Information 6, 60 (2020), arXiv:1904.02214 [quant-ph].
- [8] R. Sweke, J.-P. Seifert, D. Hangleiter, and J. Eisert, On the Quantum versus Classical Learnability of Discrete Distributions, Quantum 5, 417 (2021), arXiv:2007.14451 [quant-ph].
- [9] J. Tian, X. Sun, Y. Du, S. Zhao, Q. Liu, K. Zhang, W. Yi, W. Huang, C. Wang, X. Wu, M.-H. Hsieh, T. Liu, W. Yang, and D. Tao, Recent Advances for Quantum Neural Networks in Generative Learning, IEEE Transactions on Pattern Analysis and Machine Intelligence, 1 (2023).
- [10] M. H. Amin, E. Andriyash, J. Rolfe, B. Kulchytskyy, and R. Melko, Quantum Boltzmann Machine, Physical Review X 8, 021050 (2018).
- [11] M. Benedetti, J. Realpe-Gómez, R. Biswas, and A. Perdomo-Ortiz, Quantum-Assisted Learning of Hardware-Embedded Probabilistic Graphical Models, Physical Review X 7, 041052 (2017).
- [12] M. Kieferová and N. Wiebe, Tomography and generative training with quantum Boltzmann machines, Physical Review A 96, 062327 (2017).
- [13] S. Cheng, J. Chen, and L. Wang, Information Perspective to Probabilistic Modeling: Boltzmann Machines versus Born Machines, Entropy 20, 583 (2018), arXiv:1712.04144 [cond-mat, physics:physics, physics:quant-ph, stat].
- [14] J.-G. Liu and L. Wang, Differentiable Learning of Quantum Circuit Born Machine, Physical Review A 98, 062324 (2018), arXiv:1804.04168 [quant-ph, stat].
- [15] M. Benedetti, D. Garcia-Pintos, O. Perdomo, V. Leyton-Ortega, Y. Nam, and A. Perdomo-Ortiz, A generative modeling approach for benchmarking and training shallow quantum circuits, npj Quantum Information 5, 45 (2019), arXiv:1801.07686 [quant-ph].
- [16] J. Romero and A. Aspuru-Guzik, Variational Quantum Generators: Generative Adversarial Quantum Machine Learning for Continuous Distributions, Advanced Quantum Technologies 4, 2000003 (2021).
- [17] A. Anand, J. Romero, M. Degroote, and A. Aspuru-Guzik, Noise Robustness and Experimental Demonstration of a

- Quantum Generative Adversarial Network for Continuous Distributions, Advanced Quantum Technologies 4, 2000069 (2021).
- [18] A. Barthe, M. Grossi, S. Vallecorsa, J. Tura, and V. Dunjko, Expressivity of parameterized quantum circuits for generative modeling of continuous multivariate distributions (2024), arXiv:2402.09848 [quant-ph].
- [19] S. Lloyd and C. Weedbrook, Quantum generative adversarial learning, Physical Review Letters 121, 040502 (2018), arXiv:1804.09139 [quant-ph].
- [20] P.-L. Dallaire-Demers and N. Killoran, Quantum generative adversarial networks, Physical Review A 98, 012324 (2018), arXiv:1804.08641 [quant-ph].
- [21] C. A. Riofrio, O. Mitevski, C. Jones, F. Krellner, A. Vuckovic, J. Doetsch, J. Klepsch, T. Ehmer, and A. Luckow, A Characterization of Quantum Generative Models, ACM Transactions on Quantum Computing 5, 1 (2024).
- [22] F. J. Kiwit, M. A. Wolf, M. Marso, P. Ross, J. M. Lorenz, C. A. Riofrío, and A. Luckow, Benchmarking Quantum Generative Learning: A Study on Scalability and Noise Resilience using QUARK, KI - Künstliche Intelligenz 10.1007/s13218-024-00864-7 (2024).
- [23] H.-L. Huang, Y. Du, M. Gong, Y. Zhao, Y. Wu, C. Wang, S. Li, F. Liang, J. Lin, Y. Xu, R. Yang, T. Liu, M.-H. Hsieh, H. Deng, H. Rong, C.-Z. Peng, C.-Y. Lu, Y.-A. Chen, D. Tao, X. Zhu, and J.-W. Pan, Experimental Quantum Generative Adversarial Networks for Image Generation, Physical Review Applied 16, 024051 (2021), arXiv:2010.06201 [quant-ph].
- [24] R. Shu, X. Xu, M.-H. Yung, and W. Cui, Variational Quantum Circuits Enhanced Generative Adversarial Network (2024), arXiv:2402.01791 [quant-ph].
- [25] S. L. Tsang, M. T. West, S. M. Erfani, and M. Usman, Hybrid Quantum-Classical Generative Adversarial Network for High-Resolution Image Generation, IEEE Transactions on Quantum Engineering 4, 1 (2023).
- [26] S. Y. Chang, S. Thanasilp, B. L. Saux, S. Vallecorsa, and M. Grossi, Latent Style-based Quantum GAN for high-quality Image Generation (2024), version Number: 1.
- [27] J. Li, R. O. Topaloglu, and S. Ghosh, Quantum Generative Models for Small Molecule Drug Discovery, IEEE Transactions on Quantum Engineering 2, 1 (2021).
- [28] P.-Y. Kao, Y.-C. Yang, W.-Y. Chiang, J.-Y. Hsiao, Y. Cao, A. Aliper, F. Ren, A. Aspuru-Guzik, A. Zhavoronkov, M.-H. Hsieh, and Y.-C. Lin, Exploring the Advantages of Quantum Generative Adversarial Networks in Generative Chemistry, Journal of Chemical Information and Modeling 63, 3307 (2023).
- [29] H.-Y. Huang, R. Kueng, and J. Preskill, Predicting Many Properties of a Quantum System from Very Few Measurements, Nature Physics 16, 1050 (2020), arXiv:2002.08953 [quant-ph].
- [30] M. Arjovsky, S. Chintala, and L. Bottou, Wasserstein Generative Adversarial Networks, in *Proceedings of the 34th International Conference on Machine Learning* (PMLR, 2017) pp. 214–223, iSSN: 2640-3498.
- [31] I. Gulrajani, F. Ahmed, M. Arjovsky, V. Dumoulin, and A. Courville, Improved training of wasserstein GANs, in *Proceedings of the 31st International Conference on Neural Information Processing Systems*, NIPS'17 (Curran Associates Inc., Red Hook, NY, USA, 2017) pp. 5769–5779.
- [32] T. Salimans, I. Goodfellow, W. Zaremba, V. Cheung, A. Radford, X. Chen, and X. Chen, Improved Techniques for Training GANs, in *Advances in Neural Information Processing Systems*, Vol. 29 (Curran Associates, Inc., 2016).
- [33] A. Brock, J. Donahue, and K. Simonyan, Large Scale GAN Training for High Fidelity Natural Image Synthesis (2018), version Number: 2.
- [34] T. Karras, S. Laine, and T. Aila, A Style-Based Generator Architecture for Generative Adversarial Networks, IEEE Transactions on Pattern Analysis and Machine Intelligence 43, 4217 (2021), publisher: IEEE Computer Society.
- [35] C. K. Sønderby, J. Caballero, L. Theis, W. Shi, and F. Huszár, Amortised MAP Inference for Image Super-resolution (2016), version Number: 3.
- [36] M. Arjovsky and L. Bottou, Towards Principled Methods for Training Generative Adversarial Networks (2022).
- [37] K. Roth, A. Lucchi, S. Nowozin, and T. Hofmann, Stabilizing Training of Generative Adversarial Networks through Regularization, in *Advances in Neural Information Processing Systems*, Vol. 30 (Curran Associates, Inc., 2017).
- [38] R. Feng, D. Zhao, and Z.-J. Zha, Understanding Noise Injection in GANs, in *Proceedings of the 38th International Conference on Machine Learning* (PMLR, 2021) pp. 3284–3293, iSSN: 2640-3498.
- [39] V. Havlicek, A. D. Córcoles, K. Temme, A. W. Harrow, A. Kandala, J. M. Chow, and J. M. Gambetta, Supervised learning with quantum enhanced feature spaces, Nature 567, 209 (2019), arXiv:1804.11326 [quant-ph, stat].
- [40] M. Schuld and N. Killoran, Quantum Machine Learning in Feature Hilbert Spaces, Physical Review Letters 122, 040504 (2019).
- [41] M. Cerezo, A. Arrasmith, R. Babbush, S. C. Benjamin, S. Endo, K. Fujii, J. R. McClean, K. Mitarai, X. Yuan, L. Cincio, and P. J. Coles, Variational quantum algorithms, Nature Reviews Physics 3, 625 (2021), number: 9 Publisher: Nature Publishing Group.
- [42] M. A. Nielsen and I. L. Chuang, Quantum Computation and Quantum Information: 10th Anniversary Edition, 1st ed. (Cambridge University Press, 2012).
- [43] A. Peruzzo, J. McClean, P. Shadbolt, M.-H. Yung, X.-Q. Zhou, P. J. Love, A. Aspuru-Guzik, and J. L. O'Brien, A variational eigenvalue solver on a photonic quantum processor, Nature Communications 5, 4213 (2014).
- [44] J. Tilly, H. Chen, S. Cao, D. Picozzi, K. Setia, Y. Li, E. Grant, L. Wossnig, I. Rungger, G. H. Booth, and J. Tennyson, The Variational Quantum Eigensolver: a review of methods and best practices, Physics Reports 986, 1 (2022), arXiv:2111.05176 [quant-ph].
- [45] B. Wu, J. Sun, Q. Huang, and X. Yuan, Overlapped grouping measurement: A unified framework for measuring quantum states, Quantum 7, 896 (2023), publisher: Verein zur Förderung des Open Access Publizierens in den Quantenwissenschaften.

- [46] J. R. McClean, J. Romero, R. Babbush, and A. Aspuru-Guzik, The theory of variational hybrid quantum-classical algorithms, New Journal of Physics 18, 023023 (2016), publisher: IOP Publishing.
- [47] A. Kandala, A. Mezzacapo, K. Temme, M. Takita, M. Brink, J. M. Chow, and J. M. Gambetta, Hardware-efficient variational quantum eigensolver for small molecules and quantum magnets, Nature 549, 242 (2017).
- [48] P. Gokhale, O. Angiuli, Y. Ding, K. Gui, T. Tomesh, M. Suchara, M. Martonosi, and F. T. Chong, Minimizing State Preparations in Variational Quantum Eigensolver by Partitioning into Commuting Families (2019), arXiv:1907.13623 [quant-ph].
- [49] A. Zhao, A. Tranter, W. M. Kirby, S. F. Ung, A. Miyake, and P. J. Love, Measurement reduction in variational quantum algorithms, Physical Review A 101, 062322 (2020).
- [50] V. Verteletskyi, T.-C. Yen, and A. F. Izmaylov, Measurement optimization in the variational quantum eigensolver using a minimum clique cover, The Journal of Chemical Physics 152, 124114 (2020).
- [51] I. Hamamura and T. Imamichi, Efficient evaluation of quantum observables using entangled measurements, npj Quantum Information 6, 56 (2020).
- [52] O. Crawford, B. V. Straaten, D. Wang, T. Parks, E. Campbell, and S. Brierley, Efficient quantum measurement of Pauli operators in the presence of finite sampling error, Quantum 5, 385 (2021).
- [53] D. Wecker, M. B. Hastings, and M. Troyer, Towards Practical Quantum Variational Algorithms, Physical Review A 92, 042303 (2015), arXiv:1507.08969 [cond-mat, physics:quant-ph].
- [54] C. Hadfield, S. Bravyi, R. Raymond, and A. Mezzacapo, Measurements of Quantum Hamiltonians with Locally-Biased Classical Shadows, Communications in Mathematical Physics 391, 951 (2022).
- [55] H.-Y. Huang, R. Kueng, and J. Preskill, Efficient Estimation of Pauli Observables by Derandomization, Physical Review Letters 127, 030503 (2021), publisher: American Physical Society.
- [56] D. Ackley, G. Hinton, and T. Sejnowski, A learning algorithm for boltzmann machines, Cognitive Science 9, 147 (1985).
- [57] G. E. Hinton, A Practical Guide to Training Restricted Boltzmann Machines, in *Neural Networks: Tricks of the Trade*, Vol. 7700, edited by G. Montavon, G. B. Orr, and K.-R. Müller (Springer Berlin Heidelberg, Berlin, Heidelberg, 2012) pp. 599–619, series Title: Lecture Notes in Computer Science.
- [58] S. Kullback and R. A. Leibler, On Information and Sufficiency, The Annals of Mathematical Statistics 22, 79 (1951).
- [59] A. Borji, Pros and cons of GAN evaluation measures: New developments, Computer Vision and Image Understanding 215, 103329 (2022).
- [60] L. Dinh, J. Sohl-Dickstein, and S. Bengio, Density estimation using Real NVP (2016), version Number: 3.
- [61] J. Ho, X. Chen, A. Srinivas, Y. Duan, and P. Abbeel, Flow++: Improving Flow-Based Generative Models with Variational Dequantization and Architecture Design (2019), version Number: 2.
- [62] Y. Song, J. Sohl-Dickstein, D. P. Kingma, A. Kumar, S. Ermon, and B. Poole, Score-Based Generative Modeling through Stochastic Differential Equations (2020), version Number: 2.
- [63] L. V. Kantorovich, Mathematical Methods of Organizing and Planning Production, Management Science 6, 366 (1960).
- [64] X. Bonet-Monroig, H. Wang, and A. Pérez-Salinas, Verifying randomness in sets of quantum states via observables (2024), arXiv:2404.16211 [quant-ph].
- [65] Y. LeCun, Y. Bengio, and G. Hinton, Deep learning, Nature 521, 436 (2015).
- [66] K. Mitarai, M. Negoro, M. Kitagawa, and K. Fujii, Quantum circuit learning, Physical Review A 98, 032309 (2018).
- [67] M. Schuld, V. Bergholm, C. Gogolin, J. Izaac, and N. Killoran, Evaluating analytic gradients on quantum hardware, Physical Review A 99, 032331 (2019).
- [68] L. Mescheder, A. Geiger, and S. Nowozin, Which Training Methods for GANs do actually Converge? (2018).
- [69] S. Jerbi, C. Gyurik, S. C. Marshall, R. Molteni, and V. Dunjko, Shadows of quantum machine learning, Nature Communications 15, 5676 (2024).
- [70] H.-Y. Huang, R. Kueng, G. Torlai, V. V. Albert, and J. Preskill, Provably efficient machine learning for quantum many-body problems, Science 377, eabk3333 (2022).
- [71] H.-Y. Huang, M. Broughton, M. Mohseni, R. Babbush, S. Boixo, H. Neven, and J. R. McClean, Power of data in quantum machine learning, Nature Communications 12, 2631 (2021), arXiv:2011.01938 [quant-ph].
- [72] G. Li, Z. Song, and X. Wang, VSQL: Variational Shadow Quantum Learning for Classification, Proceedings of the AAAI Conference on Artificial Intelligence 35, 8357 (2021).
- [73] A. Basheer, Y. Feng, C. Ferrie, and S. Li, Alternating Layered Variational Quantum Circuits Can Be Classically Optimized Efficiently Using Classical Shadows, Proceedings of the AAAI Conference on Artificial Intelligence 37, 6770 (2023).
- [74] Q. Wang, S. R. Kulkarni, and S. Verdu, Divergence Estimation for Multidimensional Densities Via \$k\$-Nearest-Neighbor Distances, IEEE Transactions on Information Theory 55, 2392 (2009).
- [75] J. R. McClean, S. Boixo, V. N. Smelyanskiy, R. Babbush, and H. Neven, Barren plateaus in quantum neural network training landscapes, Nature Communications 9, 4812 (2018).
- [76] M. Ragone, B. N. Bakalov, F. Sauvage, A. F. Kemper, C. Ortiz Marrero, M. Larocca, and M. Cerezo, A Lie algebraic theory of barren plateaus for deep parameterized quantum circuits, Nature Communications 15, 7172 (2024).
- [77] X. Bonet-Monroig, H. Wang, D. Vermetten, B. Senjean, C. Moussa, T. Bäck, V. Dunjko, and T. E. O'Brien, Performance comparison of optimization methods on variational quantum algorithms, Physical Review A 107, 032407 (2023), arXiv:2111.13454 [quant-ph].
- [78] S.-X. Zhang, J. Allcock, Z.-Q. Wan, S. Liu, J. Sun, H. Yu, X.-H. Yang, J. Qiu, Z. Ye, Y.-Q. Chen, C.-K. Lee, Y.-C. Zheng, S.-K. Jian, H. Yao, C.-Y. Hsieh, and S. Zhang, TensorCircuit: a Quantum Software Framework for the NISQ Era, Quantum 7, 912 (2023).
- [79] P. Kidger and C. Garcia, Equinox: neural networks in JAX via callable PyTrees and filtered transformations (2021),

- arXiv:2111.00254.
- [80] J. Bradhury, R. Frostig, P. Hawkins, and M. James Johnson, JAX: composable transformations of Python+NumPy programs (2018).
- [81] M. Douze, A. Guzhva, C. Deng, J. Johnson, G. Szilvasy, P.-E. Mazaré, M. Lomeli, L. Hosseini, and H. Jégou, The Faiss library (2024), arXiv:2401.08281.
- [82] K. He, X. Zhang, S. Ren, and J. Sun, Delving Deep into Rectifiers: Surpassing Human-Level Performance on ImageNet Classification, in 2015 IEEE International Conference on Computer Vision (ICCV) (IEEE, Santiago, Chile, 2015) pp. 1026–1034.

Appendix A: Pseudocodes for Training Methods

We provide pseudocodes for the three variants of OT-EVS training, with differences highlighted in blue.

Algorithm 1 Joint

Require: The gradient penalty coefficient λ , the number of critic parameters \boldsymbol{w} updates per one model iteration $N_{\boldsymbol{w}}$, the batch size B, Adam hyperparameters for quantum circuit, observable and critic parameters $(\gamma^{\boldsymbol{\theta}}, \beta_1^{\boldsymbol{\theta}}, \beta_2^{\boldsymbol{\theta}}, \gamma^{\boldsymbol{\alpha}}, \beta_1^{\boldsymbol{\alpha}}, \beta_2^{\boldsymbol{\alpha}}, \gamma^{\boldsymbol{w}}, \beta_1^{\boldsymbol{w}}, \beta_2^{\boldsymbol{w}})$. Require: Initial quantum circuit, observable and critic parameters $(\boldsymbol{w}_0, \boldsymbol{\theta}_0, \boldsymbol{\alpha}_0)$.

```
1: while (\theta, \alpha) has not converged do
                       for t=1,\ldots,N_{\boldsymbol{w}} do
   3:
                                  for i = 1, \dots, B do
                                            Sample real data x^{(i)} \sim \mathbb{Q}, latent variable z^{(i)} \sim \mathbb{P}_z, a random number \epsilon \sim U[0,1].
   4:
                                            \tilde{\boldsymbol{x}}^{(i)} \leftarrow G_{\boldsymbol{\theta}, \boldsymbol{\alpha}}(\boldsymbol{z}^{(i)})
    5:
                                            \hat{\boldsymbol{x}}^{(i)} \leftarrow \epsilon \boldsymbol{x}^{(i)} + (1 - \epsilon) \tilde{\boldsymbol{x}}^{(i)}
   6:
   7:
                                \mathcal{L}_{C} \leftarrow \frac{1}{B} \sum_{i=1}^{B} \left[ D_{\boldsymbol{w}}(\tilde{\boldsymbol{x}}^{(i)}) - D_{\boldsymbol{w}}(\boldsymbol{x}^{(i)}) + \lambda \left( \left\| \nabla_{\hat{\boldsymbol{x}}} D_{\boldsymbol{w}}(\hat{\boldsymbol{x}}^{(i)}) \right\|_{2} - 1 \right)^{2} \right]
    8:
                                 \boldsymbol{w} \leftarrow \operatorname{Adam}(\nabla_{\boldsymbol{w}} \mathcal{L}_C, \boldsymbol{w}, \gamma^{\boldsymbol{w}}, \beta_1^{\boldsymbol{w}}, \beta_2^{\boldsymbol{w}})
   9:
10:
                       end for
                       Sample a batch of latent variables \{\boldsymbol{z}^{(i)}\}_{i=1}^{B} \sim \mathbb{P}_{z}
11:
                       \mathcal{L}_G \leftarrow -\frac{1}{B} \sum_{i=1}^{B} D_{\boldsymbol{w}}(G_{\boldsymbol{\theta}, \boldsymbol{\alpha}}(\boldsymbol{z}^{(i)}))
12:
                       (\boldsymbol{\theta}, \boldsymbol{\alpha}) \leftarrow \operatorname{Adam}(\nabla_{\boldsymbol{\theta}, \boldsymbol{\alpha}} \mathcal{L}_G, (\boldsymbol{\theta}, \boldsymbol{\alpha}), (\gamma^{\boldsymbol{\theta}}, \gamma^{\boldsymbol{\alpha}}), (\beta_1^{\boldsymbol{\theta}}, \beta_1^{\boldsymbol{\alpha}}), (\beta_2^{\boldsymbol{\theta}}, \beta_2^{\boldsymbol{\alpha}}))
13:
14: end while
```

Algorithm 2 Asynchronous

Require: The gradient penalty coefficient λ , the number of critic parameters \boldsymbol{w} updates per one model iteration $N_{\boldsymbol{w}}$, the number of observable parameters $\boldsymbol{\alpha}$ updates per one model iteration $N_{\boldsymbol{\alpha}}$, the batch size B, Adam hyperparameters for quantum circuit, observable and critic parameters $(\gamma^{\boldsymbol{\theta}}, \beta_1^{\boldsymbol{\theta}}, \beta_2^{\boldsymbol{\theta}}, \gamma^{\boldsymbol{\alpha}}, \beta_1^{\boldsymbol{\alpha}}, \beta_2^{\boldsymbol{\alpha}}, \gamma^{\boldsymbol{w}}, \beta_1^{\boldsymbol{w}}, \beta_2^{\boldsymbol{w}})$.

Require: Initial quantum circuit, observable and critic parameters $(\boldsymbol{w}_0, \boldsymbol{\theta}_0, \boldsymbol{\alpha}_0)$.

```
1: while (\theta, \alpha) has not converged do
                        for t = 1, \ldots, N_w do
                                    for i = 1, \dots, B do
                                                Sample real data \mathbf{x}^{(i)} \sim \mathbb{Q}, latent variable \mathbf{z}^{(i)} \sim \mathbb{P}_z, a random number \epsilon \sim U[0,1].
    4:
                                                \tilde{\boldsymbol{x}}^{(i)} \leftarrow G_{\boldsymbol{\theta}, \boldsymbol{\alpha}}(\boldsymbol{z}^{(i)})
    5:
                                               \hat{\boldsymbol{x}}^{(i)} \leftarrow \epsilon \boldsymbol{x}^{(i)} + (1 - \epsilon) \tilde{\boldsymbol{x}}^{(i)}
   6.
    7:
                                   \mathcal{L}_C \leftarrow \frac{1}{B} \sum_{i=1}^{B} \left[ D_{\boldsymbol{w}}(\hat{\boldsymbol{x}}^{(i)}) - D_{\boldsymbol{w}}(\boldsymbol{x}^{(i)}) + \lambda \left( \left\| \nabla_{\hat{\boldsymbol{x}}} D_{\boldsymbol{w}}(\hat{\boldsymbol{x}}^{(i)}) \right\|_2 - 1 \right)^2 \right]
    8:
                                    \boldsymbol{w} \leftarrow \operatorname{Adam}(\nabla_{\boldsymbol{w}}^{\mathsf{L}} \mathcal{L}_C, \boldsymbol{w}, \gamma^{\boldsymbol{w}}, \beta_1^{\boldsymbol{w}}, \beta_2^{\boldsymbol{w}})
   9:
10:
                        end for
                        Sample a batch of latent variables \{z^{(i)}\}_{i=1}^{B} \sim \mathbb{P}_{z}.
11:
                        for j = 1, ..., N_{\alpha} do

\mathcal{L}_{G} \leftarrow -\frac{1}{B} \sum_{i=1}^{B} D_{\boldsymbol{w}}(G_{\boldsymbol{\theta}, \alpha}(\boldsymbol{z}^{(i)}))
\boldsymbol{\alpha} \leftarrow \operatorname{Adam}(\nabla_{\boldsymbol{\alpha}} \mathcal{L}_{G}, \boldsymbol{\alpha}, \gamma^{\alpha}, \beta_{1}^{\alpha}, \beta_{2}^{\alpha})
12:
13:
14:
15:
                         \mathcal{L}_G \leftarrow -\frac{1}{B} \sum_{i=1}^B D_{\boldsymbol{w}}(G_{\boldsymbol{\theta}, \boldsymbol{\alpha}}(\boldsymbol{z}^{(i)}))
16:
                        \boldsymbol{\theta} \leftarrow \operatorname{Adam}(\nabla_{\boldsymbol{\theta}} \mathcal{L}_G, \boldsymbol{\theta}, \gamma^{\boldsymbol{\theta}}, \beta_1^{\boldsymbol{\theta}}, \beta_2^{\boldsymbol{\theta}})
17:
18: end while
```

Algorithm 3 Decoupled

Require: The gradient penalty coefficient λ , the number of critic parameters \boldsymbol{w} updates per iteration $N_{\boldsymbol{w}}$, the number of observable parameters $\boldsymbol{\alpha}$ updates per iteration $N_{\boldsymbol{\alpha}}$, the batch size B, Adam hyperparameters for quantum circuit, observable and critic parameters $(\gamma^{\boldsymbol{\theta}}, \beta_1^{\boldsymbol{\theta}}, \beta_2^{\boldsymbol{\theta}}, \gamma^{\boldsymbol{\alpha}}, \beta_1^{\boldsymbol{\alpha}}, \beta_2^{\boldsymbol{\alpha}}, \gamma^{\boldsymbol{w}}, \beta_1^{\boldsymbol{w}}, \beta_2^{\boldsymbol{w}})$.

Require: Initial quantum circuit, observable and critic parameters $(\boldsymbol{w}_0, \boldsymbol{\theta}_0, \boldsymbol{\alpha}_0)$.

```
1: while (\theta, \alpha) has not converged do
    2.
                         for t = 1, \ldots, N_{\alpha} do
                                      for t = 1, \ldots, \lceil N_{\boldsymbol{w}}/N_{\boldsymbol{\alpha}} \rceil do
   4:
                                                 for i = 1, \ldots, B do
                                                             Sample real data x^{(i)} \sim \mathbb{Q}, latent variable z^{(i)} \sim \mathbb{P}_z, a random number \epsilon \sim U[0,1]
    5:
                                                             \tilde{\boldsymbol{x}}^{(i)} \leftarrow G_{\boldsymbol{\theta}, \boldsymbol{\alpha}}(\boldsymbol{z}^{(i)})
    6:
                                                             \hat{\boldsymbol{x}}^{(i)} \leftarrow \epsilon \boldsymbol{x}^{(i)} + (1 - \epsilon) \tilde{\boldsymbol{x}}^{(i)}
    7:
    8:
                                                \mathcal{L}_C \leftarrow \frac{1}{B} \sum_{i=1}^{B} \left[ D_{\boldsymbol{w}}(\hat{\boldsymbol{x}}^{(i)}) - D_{\boldsymbol{w}}(\boldsymbol{x}^{(i)}) + \lambda \left( \left\| \nabla_{\hat{\boldsymbol{x}}} D_{\boldsymbol{w}}(\hat{\boldsymbol{x}}^{(i)}) \right\|_2 - 1 \right)^2 \right]
   9:
                                                 \boldsymbol{w} \leftarrow \operatorname{Adam}(\nabla_{\boldsymbol{w}}^{\mathsf{L}} \mathcal{L}_C, \boldsymbol{w}, \gamma^{\boldsymbol{w}}, \beta_1^{\boldsymbol{w}}, \beta_2^{\boldsymbol{w}})
10.
                                      end for
11:
                                      end for \mathcal{L}_G \leftarrow -\frac{1}{B} \sum_{i=1}^B D_{\boldsymbol{w}}(G_{\boldsymbol{\theta}, \boldsymbol{\alpha}}(\boldsymbol{z}))
\boldsymbol{\alpha} \leftarrow \operatorname{Adam}(\nabla_{\boldsymbol{\alpha}} \mathcal{L}_G, \boldsymbol{\alpha}, \gamma^{\boldsymbol{\alpha}}, \beta_1, \beta_2^{\boldsymbol{\alpha}})
12:
13:
14:
                         end for
                         Sample a batch of latent variables \{\boldsymbol{z}^{(i)}\}_{i=1}^{B} \sim \mathbb{P}_{z}.
15:
                         \mathcal{L}_{G} \leftarrow -\frac{1}{B} \sum_{i=1}^{B} D_{\boldsymbol{w}}(G_{\boldsymbol{\theta}, \boldsymbol{\alpha}}(\boldsymbol{z}))\boldsymbol{\theta} \leftarrow \operatorname{Adam}(\nabla_{\boldsymbol{\theta}} \mathcal{L}_{G}, \boldsymbol{\theta}, \gamma^{\boldsymbol{\theta}}, \beta_{1}^{\boldsymbol{\theta}}, \beta_{2}^{\boldsymbol{\theta}})
16:
17:
18: end while
```

Appendix B: Sample Complexity

Here, we give detailed derivation for the upper bounds on the number of measurements necessary for achieving a given small error in Wasserstein distance between shot-noise-free and shot-noise-perturbed empirical distributions produced by a generator with high confidence for both conventional and classical shadows measurement strategies. We consider shadow-frugal observables parametrization determined by the weight matrix α (Section III B). Then, any sample generated by the shot-noise-free EVS model has the following representation:

$$\boldsymbol{y}^{i} = \left[\operatorname{tr}(O_{1}\rho^{i}), \dots, \operatorname{tr}(O_{M}\rho^{i})\right]^{\top} = \left[\sum_{l=1}^{L} \boldsymbol{\alpha}_{1l} \langle P_{l}^{i} \rangle, \dots, \sum_{l=1}^{L} \boldsymbol{\alpha}_{Ml} \langle P_{l}^{i} \rangle\right]^{\top} = \boldsymbol{\alpha} \left[\langle P_{1}^{i} \rangle, \dots, \langle P_{L}^{i} \rangle\right]^{\top} = \boldsymbol{\alpha} \langle \boldsymbol{P}^{i} \rangle.$$
(B1)

The corresponding sample generated by the shot-noise-perturbed EVS model can be written as follows:

$$\tilde{\boldsymbol{y}}^{i} = \left[\hat{o}_{1}^{i}, \dots, \hat{o}_{M}^{i}\right]^{\top} = \left[\sum_{l=1}^{L} \boldsymbol{\alpha}_{1l} \langle \widehat{P_{l}^{i}} \rangle, \dots, \sum_{l=1}^{L} \boldsymbol{\alpha}_{Ml} \langle \widehat{P_{l}^{i}} \rangle\right]^{\top} = \boldsymbol{\alpha} \left[\langle \widehat{P_{1}^{i}} \rangle, \dots, \langle \widehat{P_{L}^{i}} \rangle\right]^{\top} = \boldsymbol{\alpha} \langle \widehat{\boldsymbol{P}^{i}} \rangle,$$
(B2)

where $\widehat{\langle P_l^i \rangle}$ is the estimation of the expectation of the *l*-th Pauli string for the *i*-th sample by a particular measurement strategy.

Lemma 1. Let L denote the number of k-local Pauli strings, and let B represent the batch size. Denote \mathbb{P}^B and $\tilde{\mathbb{P}}^B$ as the empirical distributions of the shot-noise-free and shot-noise-perturbed samples, respectively, generated by an OT-EVS under the shadow-frugal parameterization specified by a weight matrix α and let $\|\alpha\|_{\infty} \leq T$. Then, for any $\epsilon > 0$, the following inequality can be established for the W_1 -distance between the shot-noise-free distribution \mathbb{P}^B and the shot-noise-perturbed distribution $\tilde{\mathbb{P}}^B$:

$$\Pr(\mathcal{W}_1(\mathbb{P}^B, \widetilde{\mathbb{P}}^B) \ge \epsilon) \le \Pr\left(\bigcup_{i=1}^N \bigcup_{l=1}^L \left\{ |\langle P_l^i \rangle - \widehat{\langle P_l^i \rangle}| \ge \frac{\epsilon}{T} \right\} \right). \tag{B3}$$

Proof. Using definition of W_1 -distance and properties of the norm we have:

$$W_1(\mathbb{P}^B, \tilde{\mathbb{P}}^B) = \inf_{\pi \in S_N} \left(\frac{1}{N} \sum_{i=1}^N \| \boldsymbol{y}^i - \tilde{\boldsymbol{y}}^{\pi(i)} \|_1 \right) \le \frac{1}{N} \sum_{i=1}^N \| \boldsymbol{y}^i - \tilde{\boldsymbol{y}}^i \|_1$$
(B4)

$$= \frac{1}{N} \sum_{i=1}^{N} \|\boldsymbol{\alpha}(\langle \boldsymbol{P}^{i} \rangle - \langle \widehat{\boldsymbol{P}^{i}} \rangle)\|_{1} \le \frac{1}{N} \sum_{i=1}^{N} \|\boldsymbol{\alpha}\|_{\infty} \|\langle \boldsymbol{P}^{i} \rangle - \langle \widehat{\boldsymbol{P}^{i}} \rangle\|_{\infty}$$
(B5)

$$\leq \frac{T}{N} \sum_{i=1}^{N} \max_{l} |\langle P_{l}^{i} \rangle - \widehat{\langle P_{l}^{i} \rangle}|. \tag{B6}$$

Taking into account probability inequality:

$$\Pr(\mathcal{W}_1(\mathbb{P}^B, \widetilde{\mathbb{P}}^B) \ge \epsilon) \le \Pr\left(\frac{1}{N} \sum_{i=1}^N \max_l |\langle P_l^i \rangle - \widehat{\langle P_l^i \rangle}| \ge \frac{\epsilon}{T}\right) \le \Pr\left(\bigcup_{i=1}^N \bigcup_{l=1}^L \left\{ |\langle P_l^i \rangle - \widehat{\langle P_l^i \rangle}| \ge \frac{\epsilon}{T} \right\}\right). \tag{B7}$$

a. Conventional measurement scheme

Theorem 2 (Total Number of Measurements for Conventional Measurement Scheme). Let L be the number of k-local Pauli strings whose expectation values are to be estimated. Let B be the batch size. Let \mathbb{P}^B and $\tilde{\mathbb{P}}^B$ be the empirical distributions of a batch of shot-noise-free and shot-noise-perturbed generated samples from an OT-EVS under the shadow-frugal parameterization, specified by weight matrix α s.t. $\|\alpha\|_{\infty} \leq T$. Then, for any accuracy parameters $\epsilon, \delta \in [0,1]$, a total of

$$N_s = \left\lceil 2 \frac{T^2}{\epsilon^2} \log \left(\frac{2BL}{\delta} \right) \right\rceil BL \tag{B8}$$

measurements for the conventional measurement strategy is sufficient to ensure that

$$W_1(\mathbb{P}^B, \tilde{\mathbb{P}}^B) \le \epsilon \tag{B9}$$

with probability at least $1 - \delta$.

Proof. Using Lemma 1 and Boole's inequality, we can place an upper bound on the probability for the expression involving the W_1 -distance between distributions and then impose a condition that this probability is sufficiently small:

$$\Pr(\mathcal{W}_1(\mathbb{P}^B, \tilde{\mathbb{P}}^B) \ge \epsilon) \le \Pr\left(\bigcup_{i=1}^B \bigcup_{l=1}^L \left\{ |\langle P_l^i \rangle - \widehat{\langle P_l^i \rangle}| \ge \frac{\epsilon}{T} \right\} \right) \le \sum_{i=1}^B \sum_{l=1}^L \Pr\left(\left| \hat{p}_l^i(K) - \operatorname{tr}\left(P_l \rho^i \right) \right| \ge \frac{\epsilon}{T} \right) \le \delta.$$
(B10)

For any fixed $i \in [B]$ and $l \in [L]$ we compute average over K measurements of ρ_i , where K is chosen such that:

$$\left|\hat{p}_{l}^{i}(K) - \operatorname{tr}\left(P_{l}\rho^{i}\right)\right| \leq \frac{\epsilon}{T} \quad \text{for all } 1 \leq i \leq B, \ 1 \leq l \leq L$$
 (B11)

with failure probability $\frac{\delta}{BL}$. Using Hoeffding inequality, we can compute K:

$$\Pr\left(\left|\hat{p}_{l}^{i}(K) - \operatorname{tr}\left(P_{l}\rho^{i}\right)\right| \ge \frac{\epsilon}{T}\right) \le 2\exp\left\{-\frac{2K^{2}\epsilon^{2}}{4KT^{2}}\right\} \le \frac{\delta}{BL}.$$
(B12)

Thus, $K = \left[2\frac{T^2}{\epsilon^2}\log\left(\frac{2BL}{\delta}\right)\right]$. Multiplying it by BL gives us the total number of measurements.

b. With classical shadow

Given an unknown quantum state ρ , choose a unitary U from the Pauli ensemble uniformly and apply it to the quantum state, i.e., $\rho \to U \rho U^{\dagger}$. Let a computational basis measurement outcome be $\hat{b} \in \{0,1\}^n$. The averaged mapping from ρ to the state implied by the measurement outcomes can be viewed as a quantum channel:

$$\mathcal{M}(\rho) = \mathbb{E}\left[U^{\dagger}|\hat{b}\rangle\langle\hat{b}|U\right]. \tag{B13}$$

Inverting the channel formally gives the quantum state ρ . Given a set of actual measurement outcomes, define the classical snapshot $\hat{\rho}(\hat{b}) := \mathcal{M}^{-1}\left(U^{\dagger}|\hat{b}\rangle\langle\hat{b}|U\right)$. By definition $\rho(\hat{b})$ is an unbiased estimator of ρ , i.e., $\mathbb{E}[\hat{\rho}(\hat{b})] = \rho$. For the case of random Pauli measurements, the mapping has a closed form

$$\hat{\rho}(\hat{b}) = \bigotimes_{j=1}^{n} \left(3U_j^{\dagger} | \hat{b} \rangle \langle \hat{b} | U_j - \mathbb{I} \right), \tag{B14}$$

where $\{U_j\}$ is the sequence of the random unitaries, i.e., $U = U_1 \otimes U_2 \cdots \otimes U_n$. With this, one can estimate the expectation value of observables with an unknown quantum state. The theoretical guarantee is given as follows.

Lemma 2 (restatement of Th1, p.13 and L3, p.26 from [29]). Fix a measurement primitive \mathcal{U} of randomly chosen Pauli measurements, a collection of observables P_1, \ldots, P_L , which are at most k-local Pauli strings. Fix accuracy parameters $\epsilon, \delta \in [0, 1]$. Then, a collection of

$$K = \left[68 \frac{3^k}{\epsilon^2} \log \left(\frac{2L}{\delta} \right) \right] \tag{B15}$$

independent classical shadows allow for accurately predicting expectation values of all observables via the median of means prediction, which means that:

$$|\hat{p}_l(K) - \operatorname{tr}(P_l \rho)| \le \epsilon \quad \text{for all } 1 \le l \le L$$
 (B16)

with probability at least $1 - \delta$.

Theorem 3 (Total Number of Measurements for Classical Shadow Measurement Scheme). Let L be the number of k-local Pauli strings whose expectation values are to be estimated. Let B be the batch size. Let \mathbb{P}^B and $\tilde{\mathbb{P}}^B$ be the empirical distributions of a batch of shot-noise-free and shot-noise-perturbed generated samples from an OT-EVS under the shadow-frugal parameterization, specified by weight matrix α s.t. $\|\alpha\|_{\infty} \leq T$. Then, for any accuracy parameters $\epsilon, \delta \in [0, 1]$, a total of

$$N_s = \left[68 \frac{T^2 3^k}{\epsilon^2} \log \left(\frac{2BL}{\delta} \right) \right] B \tag{B17}$$

measurements for the classical shadows measurement scheme is sufficient to ensure that

$$W_1(\mathbb{P}^B, \tilde{\mathbb{P}}^B) \le \epsilon \tag{B18}$$

with probability at least $1 - \delta$.

Proof. Using Lemma 1 and Boole's inequality, we can place an upper bound on the probability for the expression involving the W_1 -distance between distributions and then impose a condition that this probability is sufficiently small:

$$\Pr(\mathcal{W}_1(\mathbb{P}^B, \tilde{\mathbb{P}}^B) \ge \epsilon) \le \Pr\left(\bigcup_{i=1}^B \bigcup_{l=1}^L \left\{ |\langle P_l^i \rangle - \widehat{\langle P_l^i \rangle}| \ge \frac{\epsilon}{T} \right\} \right) \le \sum_{i=1}^B \Pr\left(\bigcup_{l=1}^L \left\{ \left| \hat{p}_l^i(K) - \operatorname{tr}\left(P_l^i \rho^i\right) \right| \ge \frac{\epsilon}{T} \right\} \right) \le \delta \quad (B19)$$

For any fixed $i \in [B]$, the number of measurements K for constructing shadow array is chosen such that:

$$|\hat{p}_l(K) - \operatorname{tr}(P_l \rho)| \le \frac{\epsilon}{T} \quad \text{for all } 1 \le l \le L$$
 (B20)

with failure probability $\frac{\delta}{B}$.

Using Lemma 2 we can conclude that $K = \left\lceil 68 \frac{T^2 3^k}{\epsilon^2} \log \left(\frac{2BL}{\delta} \right) \right\rceil$. Multiplying it by B gives us a total number of measurements.

Appendix C: Shot Noise Simulation

We propose an original method to approximate the shot noise in a way compatible with automatic differentiation. This method efficiently simulates the training of (OT-)EVS with finite measurements in numerical experiments.

Since both the conventional and classical shadows measurement schemes are unbiased, we model the shot noise as a zero-mean random vector $\boldsymbol{\epsilon}$ added to the shot-noise-free expectation values of Pauli strings. The shot noise is then propagated by the weight matrix $\boldsymbol{\alpha}$ to perturb the outputs of the (OT-)EVS.

The shot noise $\epsilon \sim \Lambda(|\psi\rangle, N_s)$ depends on the measurement scheme, the measured state $|\psi\rangle$ and the number of measurements N_s . It is independent of α , as we do not bias the allocation of the measurements according to α .

Let us follow the notations of the main text. We denote the shot-noise-free expectation values of Pauli strings by $(p_l)_{l=1}^L = (\langle \psi_{\theta}(z) | P_l | \psi_{\theta}(z) \rangle)_{l=1}^L$, and the shot-noise-free and shot-noise-perturbed model outputs by \boldsymbol{y} and $\tilde{\boldsymbol{y}}$ respectively, where

$$\boldsymbol{y} := \left(\left(\left\langle \psi_{\boldsymbol{\theta}}(\boldsymbol{z}) \middle| O_{\boldsymbol{\alpha},m} \middle| \psi_{\boldsymbol{\theta}}(\boldsymbol{z}) \right\rangle \right)_{m=1}^{M} \right)^{T}, \tag{C1}$$

$$\tilde{y} = y + \alpha \epsilon.$$
 (C2)

In particular, we model ϵ as a centered Gaussian random variable

$$\epsilon \sim \mathcal{N}\left(0, \frac{1}{N_s} \Sigma\left(\boldsymbol{\theta}, \boldsymbol{z}\right)\right).$$
 (C3)

Given that every measurement outcome is independent and identically distributed, the normal approximation is accurate for sufficiently large N_s due to the Central Limit Theorem.

We illustrate the compatibility of this simulation technique with automatic differentiation by the example of differentiating the generator loss

$$\mathcal{L}_G((\tilde{\boldsymbol{y}}^b)_{b=1}^B) = -\frac{1}{B} \sum_{b=1}^B D_{\boldsymbol{w}}(\tilde{\boldsymbol{y}}^{(b)})$$
(C4)

with respect to θ . We first decompose the stochastic nodes ϵ using the Reparameterization Trick [1],

$$\epsilon = \frac{1}{N_s} S \xi, \tag{C5}$$

where S is the lower triangular matrix in the Cholesky decomposition of Σ , i.e., $\Sigma = S(S)^T$, and $\boldsymbol{\xi} = \left((\xi_l)_{l=1}^L\right)^T$ is a vector of standard Gaussian random variables, i.e., $\xi_l \sim \mathcal{N}(0,1), \forall 1 \leq l \leq L$. Chain rule now suggests

$$\frac{\partial \mathcal{L}_G}{\partial \boldsymbol{\theta}} = \frac{1}{B} \sum_{b=1}^{B} \left[\frac{\partial D_{\boldsymbol{w}}}{\partial \tilde{\boldsymbol{y}}^b} \left(\frac{\partial \boldsymbol{y}^b}{\partial \boldsymbol{\theta}} + \frac{1}{N_s} \boldsymbol{\alpha} \frac{\partial S^b}{\partial \boldsymbol{y}^b} \frac{\partial \boldsymbol{y}^b}{\partial \boldsymbol{\theta}} \boldsymbol{\xi}^b \right) \right]. \tag{C6}$$

Since the stochasticity now becomes isolated in the non-parameterized end nodes $\boldsymbol{\xi}^b$, $\frac{\partial \mathcal{L}_G}{\partial \boldsymbol{\theta}}$ is compatible with automatic differentiation. Identifying the form of Σ for the two different measurement schemes remains.

For the conventional measurement scheme, since each measurement is only used for estimating the expectation value of one Pauli string, Σ is a diagonal matrix,

$$\Sigma = \operatorname{diag}\left((\sigma_l)_{l=1}^L\right),\tag{C7}$$

where the individual covariances are given by

$$(\sigma_l)^2 = 1 - (p_l)^2.$$
 (C8)

This diagonal covariance resembles the approximation method of Ref. [77]. The difference is that binomial distribution is used instead of Gaussian distribution. Binomial distribution yields an exact description of shot noise, which is well approximable by Gaussian distribution when N_s is large. Nevertheless, as binomial distribution is discrete, it is incompatible with the automatic differentiation we desire.

In contrast, for the classical shadows measurement scheme, Σ is non-diagonal. It comes from the fact that each classical shadow contributes to the estimation of the expectation values of all Pauli strings that are marginals of the measurement basis [55]. That is, a measurement performed in the measurement basis $Q = \bigotimes_{\iota=1}^n Q^{\iota}$ contributes to the estimation of $\langle P \rangle = \langle \bigotimes_{\iota=1}^n P^{\iota} \rangle$ when $P^{\iota} \in \{Q^{\iota}, 1\}, \forall 1 \leq \iota \leq n$, and not otherwise. Therefore, the shot noise on different Pauli strings is generally correlated. From Ref. [29] (Equation S9, 10, 35, 36, 50), we can derive the covariance matrix elements below

$$(\Sigma)_{i,j}^{2} = \underset{U \sim \text{Cl}(2^{n})}{\mathbb{E}} \sum_{x \in \{0,1\}^{n}} \left| \langle x|U|\psi_{\theta}(\boldsymbol{z}) \rangle \right|^{2} \langle x|U\mathcal{M}^{-1}(P_{i})U^{\dagger}|x\rangle \langle x|U\mathcal{M}^{-1}(P_{j})U^{\dagger}|x\rangle - p_{i}p_{j}$$

$$= \left(\prod_{\iota=1}^{n} f(P_{i}^{\iota}, P_{j}^{\iota}) \right) p_{ij} - p_{i}p_{j},$$
(C9)

where $p_{ij} = \langle \psi_{\theta}(z) | P_i P_j | \psi_{\theta}(z) \rangle$ and

$$f(P_i^{\iota}, P_j^{\iota}) = \begin{cases} 0 & \text{if } (P_i^{\iota} \neq P_j^{\iota}) \text{ and } (P_i^{\iota} \neq \mathbb{I}) \text{ and } (P_i^{\iota} \neq \mathbb{I}) \\ 1 & \text{if } ((P_i^{\iota} \neq P_j^{\iota}) \text{ and } ((P_i^{\iota} = \mathbb{I}) \text{ or } (P_j^{\iota} = \mathbb{I}))) \text{ or } (P_i^{\iota} = P_j^{\iota} = \mathbb{I}) \\ 3 & \text{if } (P_i^{\iota} = P_j^{\iota} \neq \mathbb{I}) \end{cases}$$
(C10)

We remark that since the observables P_iP_j are up to 2k-local, the cost for simulating the shot noise in the classical shadows measurement scheme is always higher than that of the conventional measurement scheme.

Appendix D: Numerical Experimental Setup

We use the Python package Tensorcircuit [78] for constructing quantum circuits, Equinox [79] for constructing the remaining architecture of the generator and the critic, Jax [80] for the simulation of training and sampling and FAISS [81] for the k-NN subroutine in the KLD estimator [74]. We perform all experiments on a cluster of NVIDIA RTX2080 GPUs.

This stack allows fast training and sampling with parallelized expectation value estimation over the Pauli strings and the batch dimension. Our simulations are, however, GPU memory bounded. We notice that the GPU memory consumption scales not only in the number of qubits n, the number of Pauli strings L, and the batch size B but also significantly in the number of quantum circuit parameters θ because of automatic differentiation. Simulations of

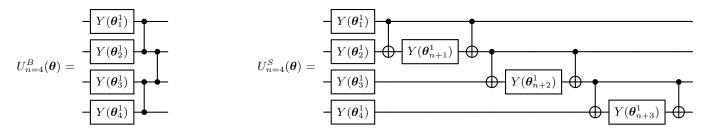


Figure 4. The circuit diagrams for one layer of brickwork ansatz (left) and one layer of sequential ansatz (right) for 4 qubits.

the shadow measurement scheme, for which the expectation values of 2k-local observables need to be computed for variance approximation (Appendix C), consume more memory than those of the conventional measurement scheme by an asymptotic factor of n^k . Limited by GPU memory, we can not simulate the classical shadows measurement scheme for larger models in Section IV, but only the conventional measurement scheme.

The two circuits we consider both consist of two parts: latent variable embedding and variational ansatz. The circuit diagrams for one layer of sequential ansatz (denoted by U^S) and one layer of brickwork ansatz (denoted by U^B) are shown in Figure 4. We consider different combinations of latent variable embedding strategies and variational ansatz. For the illustrative example of Section V A, we use

$$U^S \bigotimes_{j=1}^n X(z_2) U^S \bigotimes_{j=1}^n X(z_1).$$

For the sequential and brickwork circuits in Section VB and VC, we use

$$(U^S)^{N_l} \bigotimes_{j=1}^n Z_j(z_2) \bigotimes_{j=1}^n X_j(z_1)$$
 and $(U^B)^{N_l} \bigotimes_{\substack{j=1 \ i \text{ odd}}}^n X_j(z_1) \bigotimes_{\substack{k=1 \ k \text{ even}}}^n X_k(z_2).$

For all experiments, we generate the target distribution described as follows. We add some structure to the model parameters to ensure that the target distribution is sufficiently distinguished from pure Gaussian noises. The quantum circuit parameters are drawn from the convolution of an individual Gaussian distribution $\mathcal{N}(0, \pi/8)$ with a shared uniform distribution on $[-\pi, \pi)$. The observable parameters are randomly chosen such that for each $m \in M$, 3 of the L terms are randomly set to have values 1, 4, 9 respectively, with all other terms being 0. We chose a training dataset of 4096.

For training, the critic network architecture is taken from Ref [31] (Section 3), which consists of three hidden dense layers with 512 neurons and RELU activation function between layers. We tested that it outperforms smaller architectures but did not try bigger architectures. For initialization, the quantum circuit parameters are drawn from the uniform distribution on $[-\pi, \pi)$, and the observable and critic parameters are set according to the Kaiming Initialisation [82]. In all experiments, we consider $N_{\boldsymbol{w}} = N_{\boldsymbol{\alpha}} = 5$. The other hyperparameters for the WGAN algorithm and the Adam optimizer are searched based on a randomized grid search, with results summarized in Table II. For a fair comparison, we let all runs in each experiment (across all three WGAN variants and measurement schemes for Section VB, or across three models and circuit depths in VC) share the same hyperparameters. We perform 50k iterations for training and use 2048 samples (maximum allowed by FAISS [81]) from the generator distribution and the target distribution for evaluation every 200 iterations.

Table II. List of hyperparameters used in Section V. We perform hyperparameter optimization by random grid search for each experiment. All runs in each experiment (for all WGAN variants, all measurement schemes, or all circuit depths, when applicable) share the same hyperparameters.

			WGAN Hyperparameters											
		$\overline{\lambda}$	$N_{m{w}}$	N_{α}	В	$\gamma^{m{ heta}}$	β_1^{θ}	β_2^{θ}	γ^{α}	β_1^{α}	β_2^{α}	γ^{w}	$\beta_1^{\boldsymbol{w}}$	$\beta_2^{\boldsymbol{w}}$
Sec. VA		0.1	5	5	256	10^{-3}	0	0.9	10^{-4}	0.9	0.9	10^{-4}	0.5	0.9
	Seq.(C1)	0.1	5	5	256	10^{-3}	0	0.99	10^{-4}	0	0.9	10^{-4}	0.9	0.99
	Seq.(C2)	0.1	5	5	256	10^{-3}	0	0.5	10^{-4}	0	0.9	10^{-4}	0.5	0.9
Sec. VB	Seq.(C3)	0.1	5	5	256	10^{-2}	0.5	0.5	10^{-4}	0.5	0.9	10^{-4}	0.5	0.9
	Brk.(C1)	0.1	5	5	256	10^{-3}	0	0.9	10^{-4}	0	0.99	10^{-4}	0	0.99
	Brk.(C2)	0.1	5	5	256	10^{-3}	0	0.5	10^{-4}	0	0.9	10^{-4}	0.5	0.9
	Brk.(C3)	0.1	5	5	256	10^{-2}	0.5	0.5	10^{-4}	0	0.5	10^{-4}	0.5	0.9
Sec. VC	Seq.	0.1	5	5	256	10^{-3}	0	0.5	10^{-4}	0	0.9	10^{-4}	0.5	0.9
	Brk.	0.1	5	5	256	10^{-3}	0	0.5	10^{-4}	0	0.9	10^{-4}	0.5	0.9

Appendix E: Additional Figures

We provide here some additional results of the numerical experiments described in Section V.

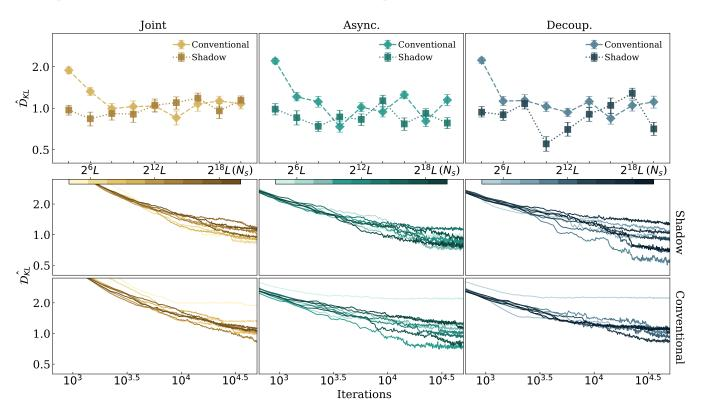


Figure 5. Supplementary result to Section VB. brickwork ansatz at small configuration. The top graphs show the interquartile mean and bootstraped 95% confidence intervals over 20 trials for the estimated KL-divergences at 50k iterations for the three WGAN variants, with different measurement configurations. The bottom graphs show the corresponding interquartile mean training trajectories.

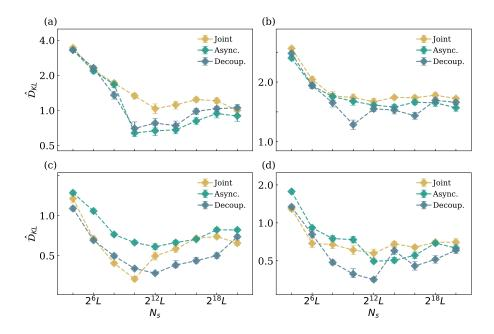


Figure 6. Supplementary result to Section VB. Only the conventional measurement scheme is considered for these configurations. (a) sequential ansatz at the deeper configuration, (b) brickwork ansatz at the deeper configuration, (c) sequential ansatz at the wider configuration, and (d) brickwork ansatz at the wider configuration are shown, respectively. All graphs show the interquartile mean and bootstraped 95% confidence intervals over 20 trials for the estimated KL-divergences at 50k iterations for the three WGAN variants, with different measurement configurations.